LIVERPOOL
JOHN MOORES
UNIVERSITY

# Faculty Research Day

# Wednesday

# 15th May 2024

# Conference Papers

# Salih Abdulqader

# Postgraduate Researcher

# School of Civil Engineering and Built Environment

# Development of a configurable microwave system for characterisation of selected substances on absorbent materials

**Salih Abdulqader[1*], Magomed Muradov[1], Patryk Kot[1], Andy Shaw[1] and Khalid Hashim[1]**

[1]Built Environment and Sustainable Technologies Research Institute (BEST), Liverpool John Moores University, Byrom Street, Liverpool, L3 3AF, United Kingdom.

*Correspondence: S.Abdulqader@2016.ljmu.ac.uk

**Abstract:** In recent years, there has been significant increase in the commercial utilisation of chemical substances (e.g., pesticides, insecticides, herbicides, and others) across various sectors. Increases can be attributed to the role of these chemical substances in enhancing the quality and quantity of products. Pesticides are detrimental and destructive to human health and the environment if overused, various techniques have been developed for monitoring the pesticides. However, they often lack capabilities like being non-destructive, cost-effective, in situ, and real-time. This study aims to design and develop a novel non-destructive configurable microwave sensor for characterising pesticides deposited on absorbent building materials. The proposed study examined the propagation of electromagnetic waves through the concrete blocks and their interaction with pesticides. The results present significant changes in $S_{11}$ magnitude and frequency when water and different weedkiller concentrations (25%, 50%, 75%, 100%) were introduced to the designed sensor. Additionally, a good correlation was observed between $S_{11}$ magnitude and weedkiller concentrations at 2.28 GHz before ($R^2 = 0.687$, $R^2 = 0.936$, $R^2 = 0.708$, $R^2 = 0.955$) and after complex subtraction ($R^2 = 0.889$, $R^2 = 0.956$, $R^2 = 0.624$, $R^2 = 0.988$).

## 1. Introduction

Currently, the economic market of pesticides is expanding rapidly across various sectors due to their ability to enhance product quality and increase productivity. However, concerns are rising over the harmful effects of pesticides on human, animal health and the environment. Pesticides encompass a wide range of substances intended to prevent, destroy, repel, or mitigate any pest. Pesticides have been linked to various diseases such as cancer, birth defects, and infertility [1]. According to the World Health Organization [WHO] classification, there are four classes: extremely, highly, moderately, and slightly dangerous, with an estimated 3 million cases of pesticide poisonings annually, and up to 220,000 deaths in developed countries. The worldwide estimated use of pesticides is about 5.2 billion pounds yearly [2]. The use of pesticides without any professional standards leads to the creation of numerous problems in the short and long term. Most (>90%) of utilised pesticides are lost when seeping into the environment and agricultural products, unable to reach the target area [3].

Therefore, many countries and organisations have a restricted level of use of pesticides and regulated strict maximum residual limits [MRLs] values for pesticides [4]. There are many developed techniques to detect pesticides such as Mass spectrometry, Electrochemical biosensors, Optical biosensors, Infrared sensors, etc [1]. However, existing techniques often suffer from being time-consuming, costly, inaccurate, and complex, unstable for on-site monitoring, and require highly skilled personnel [5].

Electromagnetic (EM) sensors are widely employed in a variety of industries, namely monitoring environmental pollution, water, and waste quality control [6], engineering material analysis, medical and agricultural food industry, chemicals, etc [7] [8]. The principle of the MW sensor technique is based on the interaction between MWs and tested materials, which alters the velocity of the signal. The permittivity of the material alters the EM signal, which causes magnitude change, resonant frequency,

or peak shifts. The change in the signal can be connected to the dielectric property of the tested object by considering how transmitted ($S_{21}$) and reflected ($S_{11}$) MW powers change at distinct frequency [9].

## 2. Methodology

An experiment was undertaken to determine the influence of weedkiller (pesticides sprayed on concrete specimens) on the EM spectrum. For this study, a MW patch-type sensor with coaxial feeding input impedances of 40 Ohms was designed using CST Studio and constructed. MW sensor is operating between 1-6 GHz frequency range and resonating at 2.4 GHz. The MW measurements were provided by S-parameters, namely the reflection coefficient ($S_{11}$). The MW sensor was designed and placed in the middle of each concrete specimens and used Rohde & Schwarz ZVL13 Vector Network Analyser (VNA) to capture S-parameters. Concrete was selected as an example of an absorbent building materials, with specimens being ((D=5cm, R5cm (R=Reverse, back), 20cm, R20cm), W=10cm, L=20cm), and were subjected to spraying with weedkiller concentrations namely 25%, 50%, 75%, 100% weedkiller/water ratio. Samples were carefully tested after one hour of spraying, with the MW sensor.
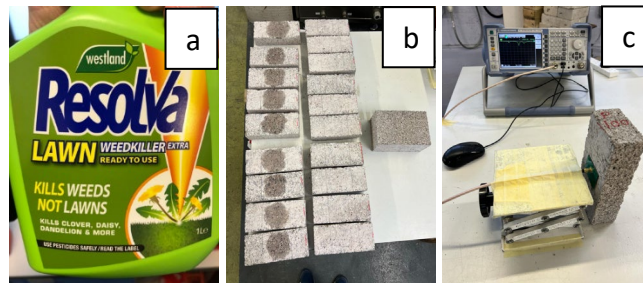


Figure 2. (a) weedkiller, (b) prepared samples, sprayed weedkiller on concrete (c) experiment setup

## 4. Results and Analysis

The results in Figure 3 shows a raw $S_{11}$ response to the changing weedkiller concentrations introduced at different specimens' thickness. There are three clear resonant peaks namely, 2.28 GHz, 3.6 GHz, 4.3 GHz, respectively.
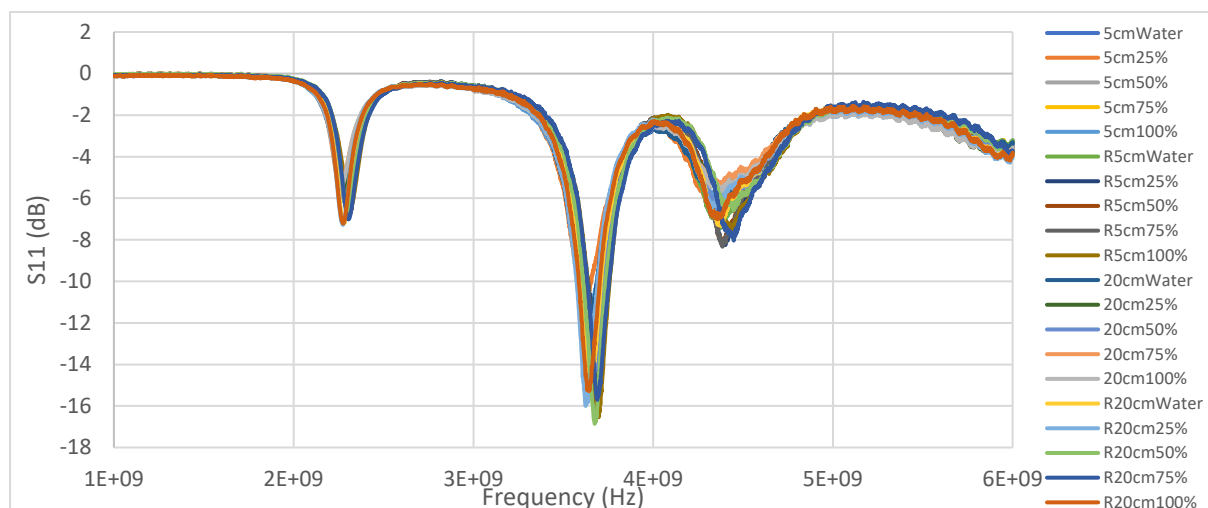


Figure 3. $S_{11}$ response for water and weedkiller concentrations using a MW sensor.

Figure 4. shows the polynomial curve fit (order 3) of the $S_{11}$ magnitude at varying weedkiller concentrations (25%, 50%, 75%, 100%) applied on concrete specimens (5cm, R5cm, 20cm, R20cm) at 2.28 GHz, showing good correlation with $R^2 = 0.687$, $R^2 = 0.936$, $R^2 = 0.708$, and $R^2 = 0.955$, respectively.
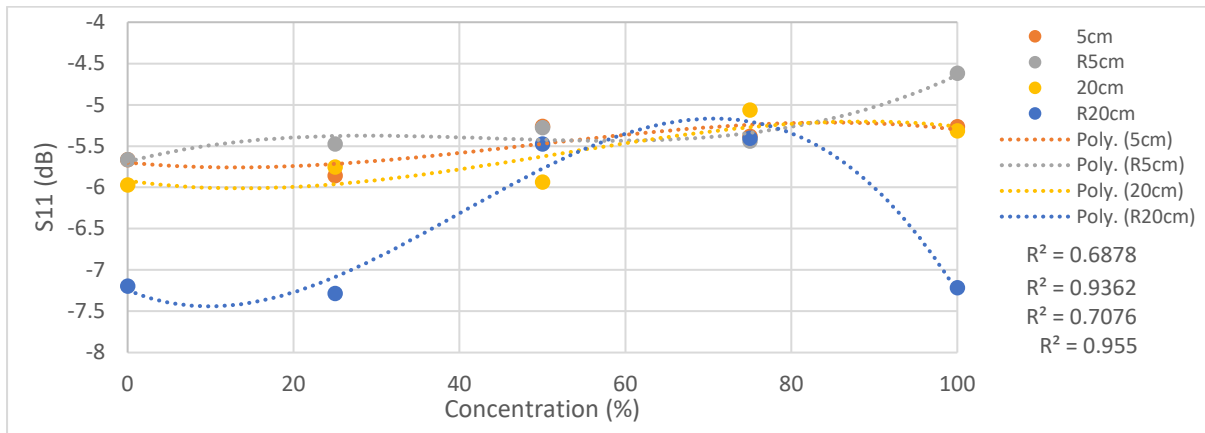


Figure 4. illustrates the correlation between S11 and water and weedkiller concentrations at 2.28 GHz.

Further work was carried out to remove any variation between concrete specimens (reduce signal background noise) the complex subtraction was carried out between unsprayed and sprayed specimens. Figure 5. presents the subtracted raw data for various weedkiller concentrations (25%, 50%, 75%, and 100%). This data demonstrates that the resonance at 2.28GHz has a larger signal to noise ratio and therefore offers better sensing capabilities for differentiating weedkiller concentrations.
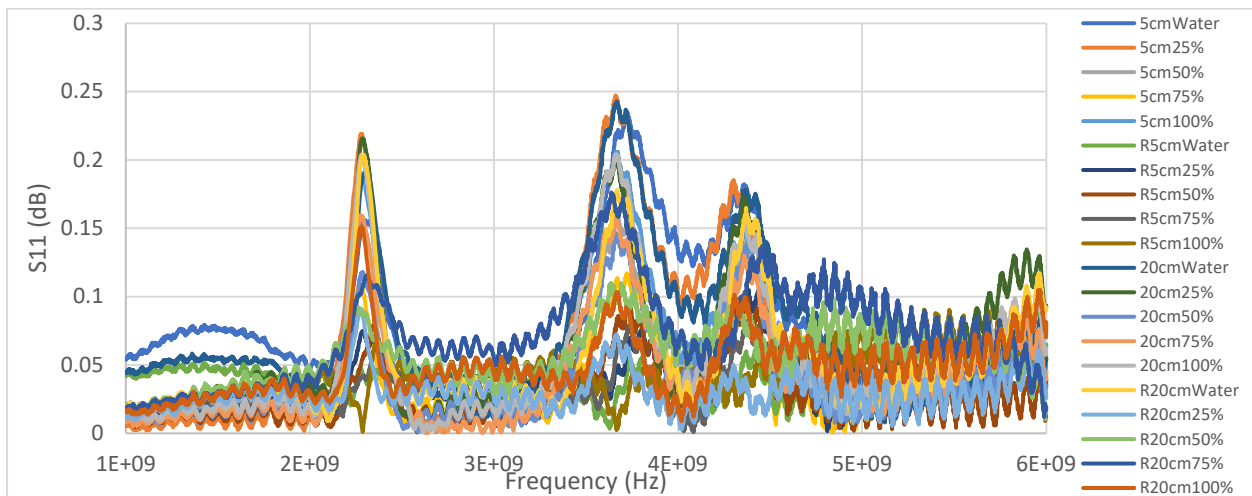


Figure 5. Complex subtraction of $S_{11}$ response for various weedkiller concentrations.

Figure 6 shows the polynomial curve fit (order 3) for complex subtraction of $S_{11}$ and weedkiller concentrations (25%, 50%, 75%, 100%) sprayed on concrete specimens (5cm, R5cm, 20cm, R20cm) at 2.28 GHz, with $R^2 = 0.889$, $R^2 = 0.956$, $R^2 = 0.624$, and $R^2 = 0.988$, respectively.
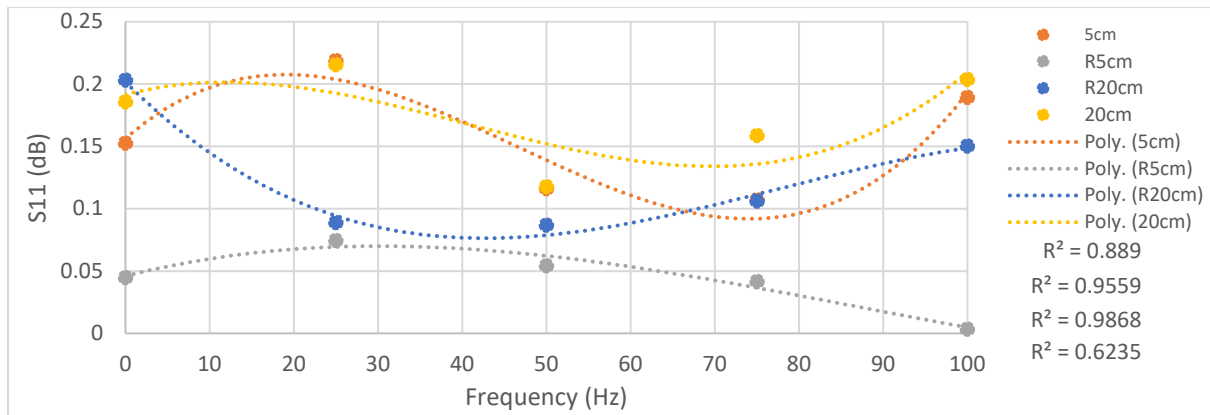
Figure 6. Correlation between complex subtraction of $S_{11}$ and weedkiller concentrations at 2.28 GHz.

### 5. Conclusion and future work

This study evaluated the capability of MW sensors to determine the pesticides deposited on absorbent building materials. An MW sensor resonating at 2.4 GHz was designed, constructed, and utilised to determine weedkiller concentration sprayed on concrete specimens. A good correlation was observed between $S_{11}$ and weedkiller concentrations at 2.28 GHz before ($R^2 = 0.687$, $R^2 = 0.936$, $R^2 = 0.708$, $R^2 = 0.955$) and after complex subtraction of the $S_{11}$ signal ($R^2 = 0.889$, $R^2 = 0.956$, $R^2 = 0.624$, $R^2 = 0.988$). This research demonstrated the potential of MW sensors as a non-destructive technique to determine pesticides in-situ and in a real-time manner.

**References:**

[1] Samsidar, A., Siddiquee, S. and Shaarani, S.M. (2018) A review of extraction, analytical and advanced methods for determination of pesticides in environment and foodstuffs.

[2] Yadav, I. and Devi, N. (2017) Pesticides Classification and Its Impact on Human and Environment. In: (ed.). pp. 140-158.

[3] Nuruzzaman, M., Rahman, M.M., Liu, Y. and Naidu, R. (2016) Nanoencapsulation, Nano-guard for Pesticides: A New Window for Safe Application. *Journal of Agricultural and Food Chemistry*, 64 (7).

[4] Belarbi, S., Vivier, M., Zaghouani, W., De Sloovere, A., Agasse, V. and Cardinael, P. (2021a) Comparison of Different d-SPE Sorbent Performances Based on Quick, Easy, Cheap, Effective, Rugged, and Safe (QuEChERS) Methodology for Multiresidue Pesticide Analyses in Rapeseeds. *Molecules*, 26 (21), 6727.

[5] Hara, T.O. and Singh, B. (2021) Electrochemical Biosensors for Detection of Pesticides and Heavy Metal Toxicants in water: Recent Trends and Progress. *ACS ES&T water*, 1 (3), 462-478.

[6] Hashim, K.S., Shaw, A., Alkhaddar, R.M., Kot, P., & Al-Shamma'a, A.I. (2021). Water purification from metal ions in the presence of organic matter using electromagnetic radiation-assisted treatment. *Journal of Cleaner Production, 280*, 124427.

[7] Muradov, M. et al. (2015) Online non-destructive monitoring of meat drying using microwave spectroscopy | IEEE conference publication | IEEE Xplore.

[8] Kot, P., Muradov, M., Ryecroft, S., Pedrola, M.O., Shaw, A., Hemingway, J., Deb, R., & Coleman, M. (2018). Identification of Optimal Frequencies to Determine Alpha-Cypermethrin Using Machine Learning Feature Selection Techniques. *2018 IEEE Congress on Evolutionary Computation(CEC)*,1-7

[9] Frau, I. et al. (2019) Functionalised Microwave Sensors for real-time monitoring of copper and zinc concentration in mining-impacted water- international journal of environmental science and technology, SpringerLink.

# Osamah Al-Hashimi
# Postgraduate Researcher
## School of Civil Engineering and Built Environment

# From landfill to lifesaver: by-products' role in restoring groundwater purity, augmented by Artificial Neural Networks

**Osamah Al-Hashimi[1,*], Khalid Hashim[1], Edward Loffill[1], Ismini Nakouti[2], and Tina Marolt Čebašek[1]**

[1]  Built Environment and Sustainable Technology Research Institute, Liverpool John Moores University, UK

[2]  Faculty of Pharmacy and Biomolecular Sciences, Liverpool John Moores University, UK.

*  Correspondence: o.a.alhashimi@2020.ljmu.ac.uk

**Abstract.** This research investigates the applicability of a re-engineered sand adsorbent derived from waste papermill sludge ash (WPSA) to remediate groundwater from antibiotic tetracycline (TC). Batch experiments and artificial neural network modelling were employed to study the adsorption of TC on the new adsorbent. The batch experiments showed that 0.3g of the manufactured adsorbent was enough to absorb as high as 10 mg/L of TC after 180 minutes at a pH of 10 and shaking at 200 rpm. The artificial neural network model successfully described the batch experiment results, exhibiting a correlation coefficient greater than 0.997. The findings demonstrate the potential of this novel adsorbent for the remediation of TC-contaminated groundwater. Additionally, the re-engineered adsorbent improves the quality of the environment by preventing the disposal of thousands of tons of waste by-products and reducing the costs associated with more complicated remediation technologies.

**Keywords.** Re-engineered sand, WPSA, Waste paper sludge ash, Arterial neural networks, Tetracycline.

## 1. Introduction

Groundwater is a vital source of freshwater for a significant portion of the global population, serving domestic, agricultural, food production, and industrial needs. Nearly one-third of the world relies on groundwater as their main potable water supply. Major cities like London, Beijing, and Buenos Aires depend heavily on groundwater resources [1]. However, the sustainability and quality of groundwater face major threats from urbanisation, agriculture, industrial activities, and climate change, which can lead to the release of contaminants such as pharmaceutical pollutants, toxic metals, hydrocarbons, pesticides, and other pollutants. Tetracyclines (TCs) are widely used antibiotics in human and veterinary medicine. A significant portion (75%) of TCs are excreted in their active form, leading to their widespread presence in various environmental sources like surface water, groundwater, drinking water, wastewater, sediments, and sludge. This widespread occurrence of TCs in the environment can cause environmental pollution and ecosystem disruption, including harmful effects on aquatic organisms like fish [2], in addition to the promotion of antibiotic resistance genes, which reduce the effectiveness of antibiotics when taken as medicine [3]. To address these issues, there is a need for developing remediation technologies; accordingly, this research aims to develop a new green adsorbent that is made from by-product waste and affordable materials such as (sand). Along with the laboratory experiments, the utilisation of artificial inelegance through the artificial neural networks is to be developed to enable accurate predictions of the behaviour of the reactive material in various environmental conditions within the limits of these experiments.

## 2. Wastepaper Sludge Ash (WPSA) in a glance

The paper industry generates substantial waste in the form of mill paper sludge from the deinking and repulping processes called wastepaper sludge ash (WPSA). The European paper industry produces approximately 11 million tons of waste per year in addition to 140,000 tonnes of WPSA produced annually in the UK [4]; much of this sludge is incinerated to recover energy, which creates a by-product of WPSA. Disposing of this ash incurs significant costs for businesses, estimated at £98.60 per tonne for disposal plus £40-45 per tonne paid to local authorities. Finding alternative uses or treatment methods for this industrial waste stream is an important challenge for the environment and the paper recycling sector.

## 3. Materials and Methods

### 3.1 Batch Experiments

Batch tests are used to determine the optimum conditions for achieving the maximum removal of TC by the developed adsorbent. These conditions include the initial concentration of the TC ($C_o$), contact time, solution's initial pH, adsorbent mass, and agitation speed. All experiments were initiated by adding 50 mL of contaminated water (V) with different $C_o$ of TC (10, 50, 100, 150, and 200 mg/L) into 250 mL flasks containing 0.1g of the new adsorbent. The solution was filtered using grade 5 Whatman filter papers to separate the solid particles. Then, a set of Hach-Lang LCK 327 cuvettes and a Hach-Lang spectrophotometer (DR3900) were used to determine the final concentration ($C_e$) of TC in the solution after filtration. The amount of TC loaded on the adsorbent ($q_e$, mg/g) was calculated using Equation (1), which is based on the mass balance principle.

1

$$q_e = (C_0 - C_e)\frac{V}{m} \qquad (1)$$

Where $qe$ is the amount of adsorbate loaded on the adsorbent (mg/g), $C_o$ and $C_e$ are the initial and final concentration of TC (mg/L), respectively, $V$ is the volume of aqueous solution (L), and $m$ is the mass of adsorbent (g).

## 3.2 Artificial Neural Networks (ANNs)

Artificial neural networks (ANNs) are computational models inspired by the human brain that excel at complex pattern recognition and mapping nonlinear relationships. They have recently gained traction in environmental applications like air/water pollution, soil remediation, and waste management due to their self-learning abilities for modelling complex nonlinear systems. ANNs consist of interconnected artificial neurons that receive inputs, process them through activation functions, and pass weighted signals between layers. In this research, ANNs predicted the removal efficiency of a new reactive media under varying environmental conditions by leveraging their ability to learn intricate nonlinear dynamics from data.

## 3.3 Materials

SAICA Paper UK Ltd, UK has provided Wastepaper sludge ash (WPSA). The WPSA sample was analysed, and its specific gravity and particle size distribution were tested. The specific gravity of the WPSA sample was 2.5, and its D50 was measured to be 13.34 µm using a Quantachrome helium pycnometer and a Laser Diffraction Particle Size Analyser (LS 12230), respectively. The Henry Cotton laboratory at Liverpool John Moores University in the UK provided the fine sand used in the coating process. The sand sample was first sieved to separate unwanted particles, and then the sand was washed and dried. The sand had a mean diameter of 1013 µm, porosity of 0.37, specific gravity of 2.685, and hydraulic conductivity of $4.719\text{x}10^{-1}$ cm/sec. All physical properties of WPSA and sand, in addition to the XRF analysis for the WPSA are shown in Table (1).

Table 31. Physical properties of the used WPSA and raw sand / XRF analysis for WPSA

| Property | WPSA | Sand | XRF analysis for Wastepaper Sludge Ash | |
|---|---|---|---|---|
| Mean diameter (µm) | 13.34 | 1013 | Calcium oxide (lime): (CaO) | 34.004 |
| pH | 12.31 | 6.76 | Chlorine: (Cl) | 8.775 |
| Specific gravity | 2.500 | 2.685 | Sulphate: (SO$_3$) | 3.144 |
| Bulk Density (Kg/m$^3$) | 561 | 1685 | Silicon dioxide (silica): (SiO$_2$) | 3.111 |
| Moisture Content (%) | 6.74 | 0.06 | Aluminium trioxide: (Al$_2$O$_3$) | 3.071 |

## 3.4 Preparation of the adsorbent

To produce 3.66 grams of coated sand, 2 grams of Waste WPSA was dissolved in 100 millilitres of deionised water and 3 millilitres of 32% HCl. The mixture was agitated for 3 hours at a speed of 200 rpm using a hot plate magnetic stirrer (Fisherbrand™, UK). Then, the solution was filtered at a No.1 Whatman filter paper, and the filtrate (rich in calcium) was mixed with 3.66 grams of FeCl$_3$, 6 millilitres of ethylene glycol, and 3.66 grams of washed sand. The mixture was then shaken for 3 hours at 200 rpm before separating the solids and drying them in a ventilated oven at 95°C for 12 hours to remove residual moisture. The final product of this process is the newly synthesised adsorbent, which is the sand coated with calcium ferric oxides.

## 4. Results and Discussion

### 4.1. ANN structure for the batch experiments

The formulation of artificial neural networks for predicting problems has originally come from the biology of the human brain [5]. In this paper, the removal of TC by the new adsorbent has been modelled using an artificial neural network (ANN) developed in MATLAB. A two-layer feedforward network with 5 inputs (adsorbent, pH, time, agitation, initial concentration), 11 hidden neurons, and removal percentage output was constructed as shown in figure (1). Various hidden layer sizes from 1-20 neurons were tested. The ANN learned complex input-output mapping from 700 data points, enabling the prediction of removal efficiency for new conditions.
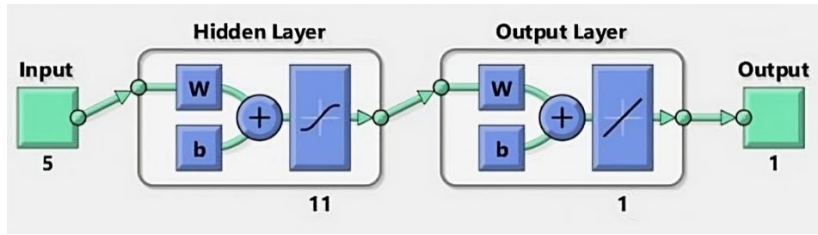
Figure 1. ANN Structure for the batch experiments.

The results from ANN have been compared with the results of batch experiments in the next section. Through the simulation, it has been found that the ANN model performs with a high degree of accuracy, suggesting its potential for use in predicting the outcomes of future experiments, with an overall regression (0.99709) proof that the excellent performance of the ANN model in simulating and predicting the efficiency of the coated sand in TC removal.

### 4.2. Batch Experiments

The experimental results, along with the ANN simulation results of the studied parameters, are explained below:

#### 4.2.1. Effect Of Initial Concentration and Contact Time

Batch experiments showed rapid TC adsorption by the new adsorbent in the first hour, then slowed afterwards to reach the maximum adsorption after 180 minutes. This behaviour could be explained by the number of active groups on the surface of the adsorbent; with time, the number of active groups is reduced due to the development of bonds between the adsorbent and the TC molecules [6]. Slower adsorption might be due to the increase in the number of occupied sites on the adsorbent's surface, while there were many available sites on the adsorbent surface at the first hour. The results also showed an inverse relationship between TC concentration and removal efficiency, where it was noticed that the removal efficiency dropped from 90% to 21% as initial TC concentration increased from 10 to 200 mg/L, respectively. When the initial concentration of TC increased, the same number of occupied sites were filled with TC, leaving the rest of TC in the aquatic environment [7], as shown in Figure (2A).
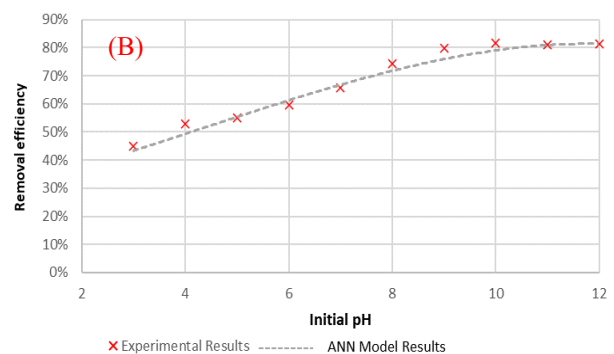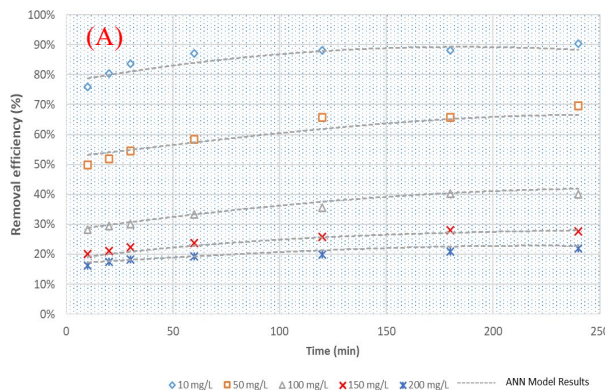
#### 4.2.2. Effects of Initial pH

The new adsorbent showed an increase in the TC removal with the rise in the pH until pH 10, then stabilised. The improvement in the TC removal is attributed to the electrostatic attraction between the adsorbent's positive surface charge above pH 5 and TC anionic species. This result complies with the results achieved by He, Pei [8], as shown in Figure (2B).

#### 4.2.3. Effects of Adsorbent Dose

Increasing the dose of the new adsorbent from 0.05 to 0.3 g/50 mL significantly boosted TC removal from 53.4% to 91.8%, respectively, due to the availability of more active sites, as illustrated in Figure (2C). However, higher doses showed no benefit due to the saturation of the surface of the new adsorbent [9].

#### 4.2.4. Effects of Agitation Speed

Increasing agitation speed from 0 to 200 rpm improved the tetracycline removal from 35% to 91.8%, respectively, as shown in Figure (2D). This increase is attributed to the fact that agitating speed promotes optimum boundary layer formation and contact between adsorbent and pollutant, improving removal efficiency. However, higher agitation speeds reduce TC removal due to the generation of turbulence [10].
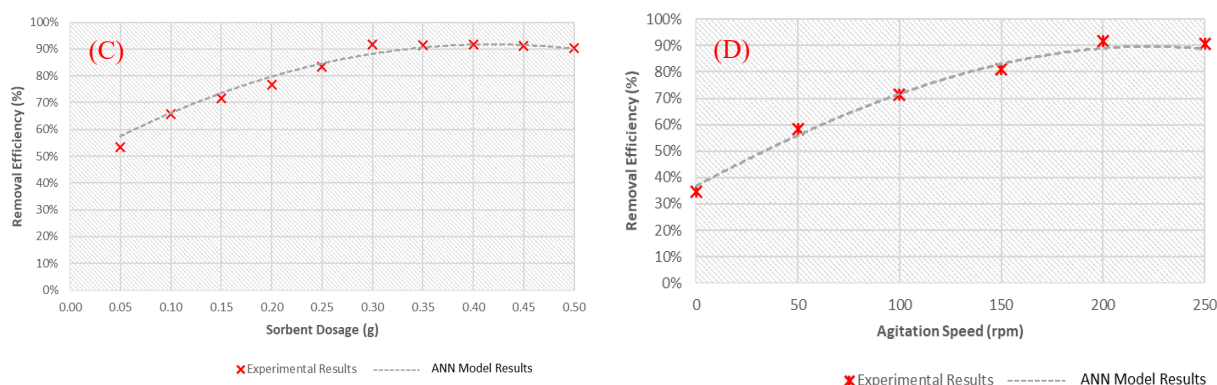


3

Figure 2. Effects of (A) contact time, B) initial pH, C) sorbent dose, and D) agitation speed on TC removal. (B, C, and D) are at 10 mg/L of TC

## 5. Conclusion

The results of the current study demonstrated the feasibility of the new adsorbent in eliminating TC antibiotics from polluted groundwater. Generally, it was noticed that the TC removal increases with the increase of pH, contact time and/or agitation speed. However, the TC removal decreases with the increase of the pollutant concentration. The results of the ANN model were highly agreed ($R^2$ 0.977) with the results of the experimental results. For future studies, it is recommended to undertake a comprehensive evaluation of the new adsorbent's effectiveness in remediating other pharmaceutical pollutants from the groundwater such Amoxicillin and Ampicillin.

## REFERENCES

1. Morris, B.L., et al., *Groundwater and its susceptibility to degradation: a global assessment of the problem and options for management.* 2003.
2. Xia, C., et al., *An effective strategy for removing tetracycline from water: Enhanced adsorption reliability and capacity by tyrosine modified layered hydroxides.* Journal of Environmental Chemical Engineering, 2023. **11**(1): p. 109172.
3. Zou, H.-Y., et al., *Antibiotic resistance genes in surface water and groundwater from mining affected environments.* Science of The Total Environment, 2021. **772**: p. 145516.
4. Fava, G., M.L. Ruello, and V. Corinaldesi, *Paper mill sludge ash as supplementary cementitious material.* Journal of materials in civil engineering, 2011. **23**(6): p. 772-776.
5. Jamali Alyani, S., et al., *Growing Co-doped TiO2 nanosheets on reduced graphene oxide for efficient photocatalytic removal of tetracycline antibiotic from aqueous solution and modeling the process by artificial neural network.* Journal of Alloys and Compounds, 2019. **799**: p. 169-182.
6. Ciğeroğlu, Z., et al., *Remediation of tetracycline from aqueous solution through adsorption on g-C3N4-ZnO-BaTiO3 nanocomposite: Optimization, modeling, and theoretical calculation.* Journal of Molecular Liquids, 2023. **369**: p. 120866.
7. Guler, U.A., E. Tuncel, and M. Ersan, *Evaluation of factors affecting tetracycline and diclofenac adsorption by agricultural soils using response surface methodology.* Environmental Progress & Sustainable Energy, 2023. **42**(1): p. e13939.
8. He, J., et al., *A new catalyst CHCP-Fe2O3 for enhanced removal of tetracycline through the Fenton-like process: Economical synthesis, catalytic performance, and practicability.* Journal of Water Process Engineering, 2023. **51**: p. 103481.
9. Althumayri, K., et al., *Enhanced Adsorption and Evaluation of Tetracycline Removal in an Aquatic System by Modified Silica Nanotubes.* ACS Omega, 2023. **8**(7): p. 6762-6777.
10. Zahoor, M., *Effect of agitation speed on adsorption of imidacloprid on activated carbon.* Journal of the Chemical Society of Pakistan, 2011. **33**(6): p. 305.

# Andrew Burgess
## Postgraduate Researcher
## School of Engineering

## A Dimensional Analysis of the Flow Behaviour of Additive Manufacturing Powders.

**Name of author:** A. Burgess
Liverpool John Moores University, 3 Byrom Street, L3 3AF, Liverpool.
E-mail address: a.burgess@2016.ljmu.ac.uk

## List of Acronyms

| Acronym | Expansion |
|---------|-----------|
| AM | Additive Manufacturing. |
| CAD | Computer Aided Design. |
| DEM | Discrete Element Method. |
| PSD | Particle Size Distribution. |
| RMS | Root Mean Square. |

### 1. Introduction

Additive Manufacturing (AM) is an emerging technique for commercial manufacturers to generate complex components more efficiently than previously thought possible. Unlike a conventional, subtractive operation in which raw materials are machined to shape, an additive approach sees parts built up layer-by-layer, one cross section at a time until the dimensions and features of the design are realised. Multiple AM methods exist, and one such flagship process is known as Powder Bed Fusion (PBF). In a PBF technique, powder is delivered to the substrate within the building chamber and dispersed by the action of a roller or blade device. Regions of this spread layer are then selectively melted by a laser or electron beam depending on the characteristics of the process, in accordance with the dimensions specified in an imported Computer Aided Design (CAD) drawing.

Despite the crucial role these powders play in the quality of the built part, their behaviour as they are processed in the build chamber remains an area of further research. In the PhD project which informs this paper, a technique to digitally model the powder flow known as the Discrete Element Method (DEM) is used. The DEM describes a range of numerical methods for the simulation of granular materials and has been recently used by researchers to create a digital twin of commercial AM powder bed systems, without incurring the costs of practical trial and error based experiments. Unlike in a continuum approach, each particle in the powder bulk is considered to be a discrete element and the code solves for the interactions between these elements to simulate the bulk powder flow. The properties of the material is assigned and the analysis is performed in the system built to replicate AM conditions.

### 2. Method

This paper proposes a novel technique to characterise the flow behaviour of metal AM powders. To achieve this, all variables which are proposed to influence the flow are stated and grouped into those which can be controlled, such as operational parameters including recoater spreading speed and powder characteristics such as the Particle Size Distribution (PSD), and processing factors which cannot, including inherent powder properties such as the morphology and chemical composition of the powder influenced by the atomisation method. A boundary of rationality is introduced that flowability is only evaluated for the delivery of the powder to the build chamber, until the point when the powder has been spread and settled immediately prior to melting. Thus, neglecting the changes in powder composition induced by thermodynamic processes.

To aid in the dimensionless analysis, the variables which influence flowability are stated in ***Table 1*** and is considered exhaustive so far as reasonably practicable.

## Table 1 - Theorised Variables Effecting the Flow of AM Powders.

| Pre-Spreading | During Spreading | Post-Spreading |
|---|---|---|
| Young's Modulus: An inherent property of the powder material. | PSD inserted to the bed. | Melting methods. |
| Density: An inherent property of the powder material. | Phase of powder processed (recycled / fresh). | Melting pattern. |
| Morphology: Depends on the atomisation process used to produce the powder. | Spreading speed. | Optical properties. |
| Porosity: Depends on the atomisation process used to produce the powder. | Spreader shape. | Thermo-Physical Properties. |
| Chemical composition and Surface Texture: Depends on the powder production process and the material selected. | Chamber environment. | |
| Time of Storage at Rest. | Moisture. | |
| Permeability: An inherent property of the powder material. | Electro-Static Charge and Interparticle forces. | |
| Delivery technique (immediately prior to spreading). | | |

To characterise the powder flow behaviour, it is necessary to perform dimensional analysis to identify the variables which are likely to effect a change in the spread layer formed. Considering the metrics previously identified to quantify a suitable powder bed for AM processing, the changes may constitute an improvement in the packing density or a segregation effect of polydisperse powders. A more qualitative inspection would be to compare the surface roughness profiles of the spread layers against a combination of input variables, such as the PSD of the powder set and the recoater velocity used to spread the powder, and then analyse the data to define the proposed spreading regimes which give rise to a smooth surface engendering favourable AM conditions, or a heterogeneous profile liable to induce an inconsistent melting pattern and thus porosity in the built component.

It is proposed from this analysis that the regimes can be defined from the variables to mathematically quantify the spreading regimes that form a smooth, transitional, and rough layer, analogous to other analytical engineering techniques such as by using the properties of fluid flow to determine a Reynold's Number which characterises laminar, transitional, and turbulent regimes.

*Table 2* assigns the dimensions to the units most commonly associated with each variable of the process outlined in *Table 1*.

**Table 2 - Units and Dimensions Associated with Each Variable of Flowability.**

| Variable | Associated units. | Dimensions. |
|---|---|---|
| Young's Modulus. | GPa | $M^1 L^{-1} T^{-2}$ |
| Density. | $\dfrac{kg}{m^3}$ | $M^1 L^{-3}$ |
| Morphology: Depends on the atomization process used to produce the powder. | μm | L |
| Porosity: Depends on the atomization process used to produce the powder. | No units. | None |
| Chemical composition and Surface Texture: Depends on the powder production process and the material selected. | Chemical composition will vary depending on alloying elements.<br><br>Surface Texture<br>nm | Chemical composition will vary depending on alloying elements.<br><br>Surface Texture:<br>L |
| Time of Storage at Rest | Seconds | T |
| Permeability: An inherent property of the powder material. | Darcy (d) | $M^1 L^1 T^{-2} I^{-2}$ |
| Delivery technique (immediately prior to spreading). | Either rainfall (acceleration due to gravity) or funnel deposition ($\frac{m}{s}$) | Rainfall:<br><br>$M^{-1} L^3 T^{-2}$<br><br>Moving Funnel:<br><br>$L^1 T^{-1}$ |
| PSD inserted to the bed. | Percentile of sizes. | L |
| Phase of powder processed (recycled / fresh). | Either cycle number, or inserted percentage of fresh powder. | None. |
| Spreading speed. | $\dfrac{m}{s}$ | $L^1 T^{-1}$ |
| Spreader Shape. | Width, length, and height. | L |
| Chamber environment. | Pa | $M^1 L^{-1} T^{-2}$ |
| Moisture. | $\dfrac{g}{m^3}$ | $M^1 L^{-3}$ |
| Electro-Static Charge and Interparticle forces. | C or N | Coulomb:<br>$M^0 L^0 T^1 I^1$<br><br>Newtons:<br>$ML^{-1} T^{-2}$ |
| Melting methods | Laser or<br>Electron Beam | Line Energy:<br>$M^1 L^1 T^{-2}$<br><br>Energy Density:<br>$M^1 L^{-1} T^{-2}$ |
| Melting pattern | Various | Various |
| Optical and Thermo-Physical properties. | Various | Various |

The following assumptions are made prior to the analysis:

- More spherical powder particles are more flowable.

- The majority of powder characterizations regarding flowability are done in the field of pharmaceuticals.

- A wide PSD is beneficial to occupy interstices in the powder bed but a narrow PSD contributes to a greater flowability.

- The recycling effect is mainly manifested by the changes to the PSD, and the more recycled the powder is the better the flowability. Recycling can almost certainly be accounted for by moisture content and PSD of the recycled sample set.

- With respect to the surface texture or the particles, elements with rougher surfaces are likely to have a propensity for mechanical interlocking and higher frictional forces, and thus behave more cohesively.

- van der Waals forces appear to be the dominant cohesion force at finer particle sizes, and for coarser particles gravitational forces are dominant. Moisture content influences capillary interactions and causes particles to bridge, thereby raising agglomerations.

- Denser and less porous particles are more flowable.

- Reducing electrostatic charges can improve powder flowability.

- Young's Modulus appears to influence particle flow at the millimetre scale but it is unknown if the same effect is observed at the micron level.

- It is assumed that the spreader shape and speed can be mathematically correlated to reduce bed degradation at higher recoater speeds, by adapting the shape of the recoater.

- Empirical evidence suggest that powder is "twice as flowable in a vacuum". It is feasible that this is due to the lack of friction forces.

With respect to how the powder parameters influences the powder bed formed, the powder profile surface roughness is one quantifiable metric of bed quality. For example, if the input parameter is the PSD, the results give a range of Root Mean Square (RMS) surface roughness values as presented in *Table 3*.

**Table 3 - Surface Roughness Results of Various Different Particle Size Distribution Sets.**

| Experiment | Particle Size Distribution (% particle diameter) | | | Overall Average Surface Roughness (μm) |
|---|---|---|---|---|
| | 40 μm | 30 μm | 20 μm | |
| 1 | 100 | 0 | 0 | 10.07 |
| 2 | 33.33 | 33.33 | 33.33 | 7.35 |
| 3 | 60 | 25 | 15 | 9.10 |
| 4 | 15 | 25 | 60 | 6.00 |
| 5 | 25 | 50 | 25 | 7.29 |
| 6 | 0 | 0 | 100 | 4.09 |
| 7 | 0 | 100 | 0 | 7.89 |

Based on the average surface roughness values generated, an example regime may resemble:

$$Smooth \ < 7.08 \, \mu m \ > Rough$$

The waveforms projected onto the $xz$ plane of the powder bed for the experiments were too similar to be compared visually. Because the particles were so small, and there are so many of them in the powder bed spreading length, taking a segment sample (such as from Experiment 1 and Experiment 6, the roughest and smoothest layers as shown in *Table 3*) was unlikely to be representative of the full powder span. For this reason, a numerical value (7.08 μm) has been proposed as the transition point in this instance between smooth and rough powder layers. Note that because the data population is small, this is fairly arbitrary and the is just selected as the mid-point between the lowest and highest surface roughness values. Applying this logic as a base concept, it could therefore be proposed that the powders generated by the PSD in each experiment can be classified as in *Table 4*.

**Table 4 - Classification of Smooth and Rough Spreading Regimes with the Input of the Particle Size Distribution.**

| Experiment | Classification |
|---|---|
| 1 | Rough |
| 2 | Slightly Rough (transitional) |
| 3 | Rough |
| 4 | Smooth |
| 5 | Slightly Rough (transitional) |
| 6 | Smooth |
| 7 | Slightly Rough (transitional) |

### 3. Discussion

This paper discussed establishing a proposed regime of powder flowability in AM systems. Based on the classification of proposed smooth and rough spreading regimes defined in ***Table 4***, the dimensional analysis could be extended to plot the influence of a range of variables on the dynamic behaviour of powder. In the case of this paper, the criteria manifesting the effect of the powder flowability has been defined as the surface roughness of the formed spread layer. However, other key performance indicators such as the segregation in the spread layer or the packing density attained could also be used either as well or instead of this metric.

By deriving the relationships mathematically, the multifaceted variables which serve to influence the quality of the formed powder bed could be discretised into multiple groups with the input properties (such as recoater speeds and PSD ranges) calibrated to optimise the powder bed for a given manufacturing operation. Thus, performing a comprehensive dimensional analysis is proposed to be a feasible route for improving the efficiency of commercial AM operations and contemporary powder based AM research projects.

# Tom Cottage
# Postgraduate Researcher
# School of Engineering

# The effect of rotor cavity shape on the mixing performance of a novel rotor-stator mixer

**T Cottage**
School of Engineering, Liverpool John Moores University.
James Parsons Building, Byrom Street, Liverpool, L3 3AF.
E-mail address: T.Cottage@2021.ljmu.ac.uk

**Abstract.**
The shape of rotor cavities in a model of the controlled deformation dynamic mixer (CDDM) is varied to create six configurations which are investigated numerically through Computational Fluid Dynamics (CFD) techniques. A 2D cross-sectional representation of an existing CDDM configuration is used as the base case and informs the dimensions of the shapes, with a sliding mesh model employed for the rotor rotation. The mixing performance of each configuration, processing water and a blob of dye, is evaluated through examination of the variance of the dye volume fraction after a process time of 1.2 seconds. It is found that a 'teardrop' shaped cavity resulted in the dye blob being more mixed than the other configurations. However, the rate of mixing for the initial stages of the simulation was better for other shape configurations, suggesting the amount of mixing time should be considered when selecting the 'best' rotor cavity shape for mixing.

**Keywords.** *Controlled Deformation Dynamic Mixer (CDDM), Computational Fluid Dynamics (CFD)*

## 1 Introduction

Rotor-stator mixers (sometimes referred to as high-shear mixers) are widely used fluid mixing devices throughout the process industries due to their inherent ability to impart the high shear rates required to mix viscous fluids effectively [1]. These mixers consist of a rotating element enclosed by a stationary sleeve in close proximity, creating narrow shear gaps and channels by which the fluid can be forced through or impinge upon. Examples exist of both batch mixers and inline mixers for this style of device. A recent novel design of inline rotor-stator mixer is the Controlled Deformation Dynamic Mixer (CDDM), which is a cavity type mixer with design features informed by the previous Cavity Transfer Mixer (CTM) [2]. The CDDM, like its predecessor the CTM, consists of a rotor shaft that features several rows of cavities and a stator sleeve that also features cavities such that these cavities are on confronting surfaces. This leads to fluid paths being formed within the gaps and around the cavities that are subject to large volumetric variations. The smallest of these being the 'shear gap' which is the section in which the inner diameter of the stator sleeve is at a minimum and the outer diameter of the rotor shaft is at a maximum and are confronting. What makes the CDDM novel compared to other inline cavity type mixers, is the ability to introduce shims to the stator sleeve, to alter the axial position relevant to the rotor [3]. This alters the fluid paths that are created and can lead to an assortment of gap sizes at the cavity edges. Figure 1 shows a 3D model of the CDDM and a demonstration of the 3 modes achieved through shim introduction.
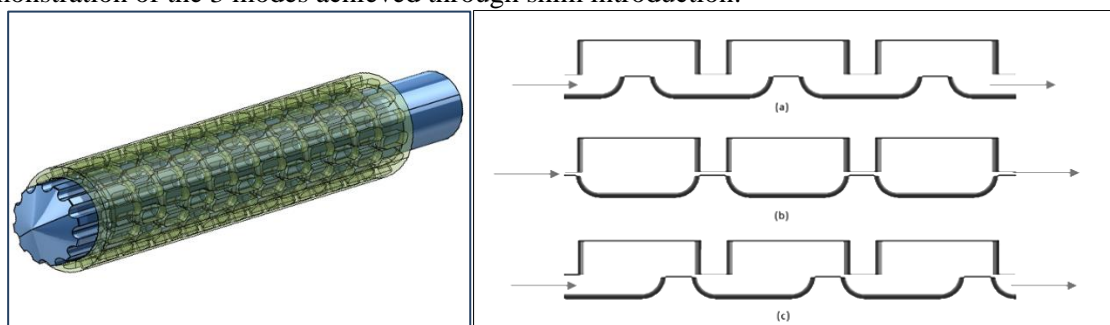


*Figure 1:A 3D CAD model of the CDDM (left), The three configurations of the CDDM, a) CTM mode, b) Full CDDM mode, c) Knife-edge mode (right).*

Computational Fluid Dynamics (CFD) is a method of numerically solving fluid flows and heat transfer problems. Inline rotor-stator mixers are inherently difficult to investigate through experimental techniques due to the fact that the regions of interest are enclosed within the tight shear gaps which in the CDDM, can be as minimal as 55 microns. For this reason, CFD offers an opportunity to investigate the flow behaviour within the equipment without the need for developing and funding complex experiments. The CDDM has not yet been investigated through CFD techniques in published work to the best of the author's knowledge.

## 2 Methodology
### 2.1 2D Geometry
The mixer geometry has been simplified to a 2D case, representing a cross-section of the CDDM at a position along the length of the mixer that captures the maximum depth of the rotor and stator cavities. Modelling the CDDM in this manner allows for the rotation to be captured but neglects the axial component of the flow. For this study, the shape of the stator cavity is maintained and the rotor cavities are modified. Figure 2 shows the 6 configurations explored. Configuration A is dimensionally accurate to the bench-top CDDM and subsequent configurations are modelled according to this with care taken to ensure that the area of the rotor including cavities is kept consistent so that mixing performance can be evaluated between cases without the need for scaling arguments.
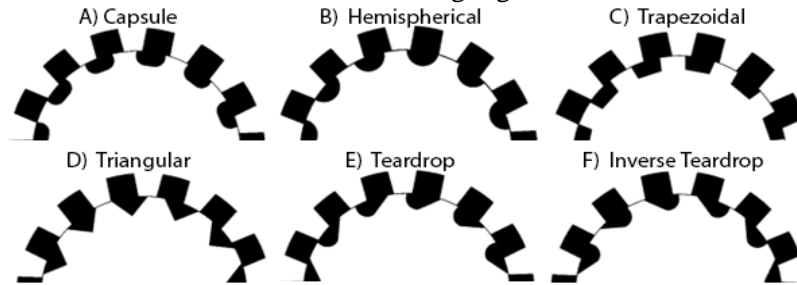


*Figure 2: A representation of the configurations of this study (only the top half shown).*

### 2.2 CFD methodology
An Unsteady Reynolds Averaged Navier Stokes (URANS) approach through ANSYS® Fluent 2022 R2 was employed. The governing equations are shown in (1) and (2) for conservation of mass and conservation of momentum respectively. Transient simulations were undertaken to allow for the tracking of the mixing behaviour through time, with a final flow time of 1.2 seconds for each configuration. A mesh independence study was conducted identifying the chosen mesh size of approximately 1E06 quadratic elements as appropriate. Mesh refinement through inflation layers [4] was employed at all boundaries to sufficiently capture the boundary layer, with a minimum of 20 cells sought across narrow gaps.

$$\frac{\partial \rho}{\partial t} + \frac{\partial (\rho u_i)}{\partial x_i} = 0 \tag{1}$$

$$\rho \left( \frac{\partial u_i}{\partial t} + u_j \frac{\partial u_i}{\partial x_j} \right) = \rho g_{x_i} - \frac{\partial p}{\partial x_i} + \mu \left( \frac{\partial^2 u_i}{\partial x_i \partial x_j} \right) \tag{2}$$

The regime was characterised through the rotational Reynolds Number ($Re_r$) shown in (3), where $\rho$ is the fluid density, $\mu$ is the fluid dynamic viscosity, $N$ is the rotor speed and $D_R$ is the rotor swept diameter. As the value of $Re_r$ is above $10^4$, this suggests a turbulent flow regime is in operation therefore the employment of a turbulence model is necessary.

$$Re_r = \frac{\rho N D_R^2}{\mu} \tag{3}$$

Through literature, the $k$-$\varepsilon$ two equation turbulence model was identified as being widely used for CFD studies of rotor-stator mixers and in one particular study, shown to capture velocity distributions and flow periodicity well in an analysis of an inline rotor-stator mixer [2]. Rotation is captured by employing the sliding mesh approach, which allows a mesh zone to be defined for each the stator and the rotor separately and the rotor allowed to rotate relative to the stationary region of the stator [5]. The rotational speed is defined as 1500 RPM and kept consistent across the models.

The mixture model [5] is employed to solve for the multiphase aspects of the flow. The working fluid is water ($\rho$ = 1000 kg m$^{-3}$ , $\mu$ = 1E-05 kg m$^{-1}$s$^{-1}$) and the inclusion of the secondary phase is completed through creating a representative dye phase with the same properties as water, allowing the mixing of a blob of this to be tracked. The dye blob represents approximately 2% of the total volume of the fluid in the mixer and is located such that it equally protrudes into a rotor cavity and opposing stator cavity.

## 3 Results and discussion

Initial validation of the results is conducted through comparison against lid driven cavity (LDC) benchmarks, by considering a single rotor cavity to be analogous to an LDC. These are well researched in literature both numerically and experimentally, and can be shown to offer the same flow characteristics to this study. This is in terms of location of generated vortices such as for hemispherical and square cavities [6], triangular and trapezoidal cavities [7] and teardrop vortex location validated through a study on flow characteristics over teardrop dimples [8]. Vorticity is plotted in Figure 3 for each configuration. It can be seen that the vortex generated in the stator cavity shows good relative agreement between all models except configuration B, the hemispherical rotor, which instead demonstrates larger regions of high intensity clockwise swirling
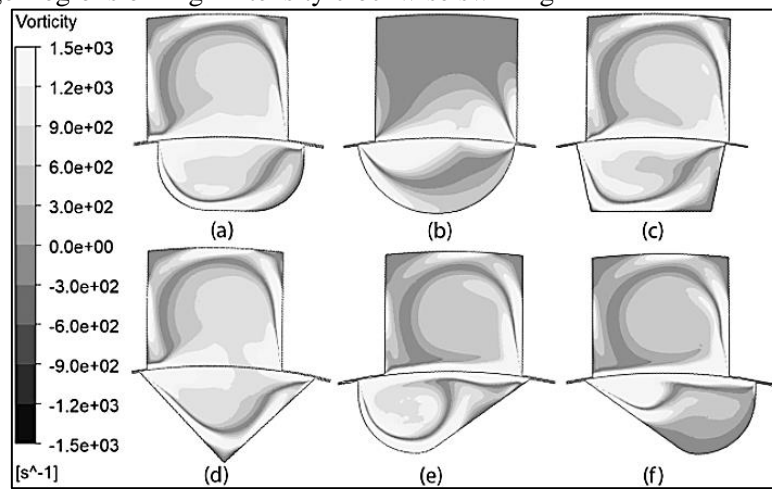


Figure 3: Vorticity contours for each configuration at t=1.2[s], showing the top most rotor and stator cavities confronting.

The volume fraction of a given phase represents the amount of that phase present in a given cell and is normalised between 0 and 1, where 0 demonstrates that none of that phase is present and 1 meaning that the cell is 100% that phase .

To evaluate the level of mixing that has occurred, the variance in the spatially average volume fraction of the dye phase is considered. The instantaneous volume fraction of the dye phase at any given point can be described by $\varphi_i = \overline{\varphi} + \varphi''$. Where $\varphi_i$ is the dye volume fraction, $\overline{\varphi}$ is the dye volume fraction spatially averaged and $\varphi''$ a fluctuating value around this average.

The statistical variance is therefore given by $\varphi''^2 = (\varphi - \overline{\varphi})^2$. Therefore, when this dye volume fraction variance is 0, the mixture can be considered to be completely mixed (i.e. The percentage of the whole domain that was initially dye, now applies to all discrete elements in the domain). Therefore, the mixing performance of a system can be evaluated through firstly, considering how close to 0 the dye volume fraction variance is after a given time. Alongside this, the rate at which the volume fraction variance reduced should be considered.

Figure 3 shows the dye volume fraction variance for each system after an equivalent flow through time. It can be seen that the system that reaches the lowest value, and is therefore considered to be better mixed, is configuration E, the teardrop rotor. This is likely due to the fact that the large surface area in the left hand side of this shape encourages a large vortex to form, which is conducive to fluid mixing. Yet the right hand side with its rapid area reduction towards the far edge allows the fluid leaving the vortex to flow freely back towards the channel. This is in contrast to the shapes such as the configuration A capsule and configuration C square, which through symmetry, have large surface areas at both sides which form multiple larger vortices that may essentially 'trap' parcels of fluid in these regions, preventing these from mixing back into the free stream.

Interestingly, configuration F, the inverse teardrop demonstrates a much quicker rate of mixing for the majority of the simulation time before being overtaken by other configurations. Configuration F also does not follow the same general trend as the other shapes, possibly due to the fact that with the clockwise rotor rotation, this asymmetric shape has a low volume at its leading edge and a large volume at the far side, which is unique amongst the six configurations.
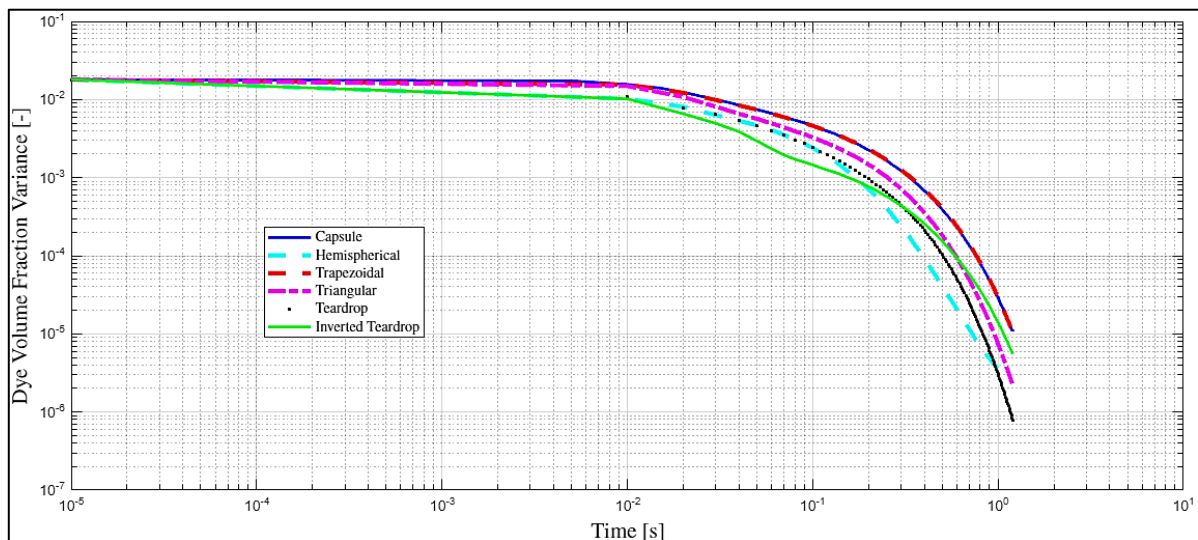


*Figure 4: Dye volume fraction variance with flow time for each CDDM rotor shape configuration.*

Considering the other configurations, the trends are shown to be roughly the same with some slight differences in the rate of mixing and the final values. The original bench-top mixer of Configuration A, behaves relatively poorly compared to other mixers however, has almost identical behaviour to the square rotor of Configuration C.

## 4 Conclusion

Given the run time set for this study, the teardrop shaped rotor of Configuration E shows the best mixing performance. However, should less time be sought for mixing, the rate of mixing may offer a better final result from the hemispherical Configuration B or the inverse teardrop Configuration F. Further investigation is required into how well these trends are maintained over longer mixing periods and whether the rotational speed effects this result. This brief study demonstrates at least, that the current design of rotor on the CDDM may not offer the best mixing performance and that CFD Future work also requires expanding these simulations to full 3D cavity shapes, to accurately capture the inherently 3D turbulent mixing behaviours, and impart further confidence that the design recommendations are correct before attempting to manufacture a new rotor.

## 5 References

1. John TP, Panesar JS, Kowalski A, Rodgers TL, P. Fonte C. Linking power and flow in rotor-stator mixers. Chem Eng Sci. 2019;207:504–15.
2. Brown CJ, IGN and KAJ. Mixing Apparatus of the CDDM- or CTM-Type, and its Use. WO/2010/091983, 2010.
3. Harvey DHS, Mothersdale T, Shchukin D, Kowalski AJ. Plant Fiber Processing Using the Controlled Deformation Dynamic Mixer. Chem Eng Technol. 2019 Aug;42(8):1566–73.
4. ANSYS. Ansys Meshing Users Guide. ANSYS, Inc.; 2022.
5. Xu S, Cheng Q, Li W, Zhang J. LDA measurements and CFD simulations of an in-line high shear mixer with ultrafine teeth. AIChE Journal. 2014 Mar 1;60(3):1143–55.
6. ANSYS. Ansys Fluent Theory Guide. ANSYS, Inc.; 2022.
7. ANSYS. Ansys Fluent Users Guide. ANSYS, Inc.; 2022.
8. Migeon C, Texier A, Pineau G. Effects of Lid-Driven Cavity Shape on the Flow Establishment Phase. J Fluids Struct. 2000;14(4):469–88.
9. An B, Guo S, Bergadà JM. Lid Driven Triangular and Trapezoidal Cavity Flow: Vortical Structures for Steady Solutions and Hopf Bifurcations. Applied Sciences (Switzerland). 2023 Jan 1;13(2).
10. Zhang Z, Xie Y, Zhang D, Xie G. Flow Characteristic and Heat Transfer for Non-Newtonian Nanofluid in Rectangular Microchannels with Teardrop Dimples/Protrusions. Open Physics. 2017 Jan 1;15(1):197–206.

# Joe Ford
# Postgraduate Researcher
# School of Engineering

# Analysis of offshore decommissioning waste management using a bayesian network.

**J.M.Ford[1], S.Loughney, E.Blanco-Davies, A.Shahroki, A.Armada Bras and J.Wang.**
Liverpool John Moores University, Liverpool, United Kingdom.
Corresponding Author E-mail address: [1] j.m.ford@2019.ljmu.ac.uk

**Abstract.** With the offshore decommissioning industry's estimated expenditure exceeding £21 billion over the next decade, this research study focuses on the handling of waste materials generated during this process. A Bayesian network, derived from prior research and publicly available data, was used to analyse the complex interactions influencing waste management decisions. The research study aims to contribute to the understanding of the handling of decommissioning waste materials. The research stresses the importance of informed decision-making to minimize environmental impact and streamline the handling of hazardous waste materials, ultimately contributing to a more sustainable decommissioning approach.

**Keywords.** Decommissioning, offshore, bayesian network.

## 1. Introduction & Background

Within the United Kingdom Continental Shelf (UKCS), once an installation has reached the end of its life, it cannot simply be left in place to rot. It must be decommissioned in line with the current United Kingdom (UK) legislation and regulations and the seabed returned to its original state. Issues arise where installations may have changed ownership, mode of operation, or, simply due to their age. Decommissioning expenditure is expected to reach at least £21 billion over the next decade. Although moves are being made to reduce this expenditure, it is expected to peak in 2032 with the ever-increasing number of aging installations (NSTA 2023).

UK legislation requires installations to be decontaminated from hazardous waste before any part can be reused or recycled. This hazardous waste must be handled, transported, and disposed of in a way that does not impact safety or the environment. Currently, there is an emphasis on reducing the volume of waste that is sent to landfill and encouragement to reuse or recycle materials wherever possible (Perks, 2012) (OGA, 2015) (Brady, 2022). This is written into decommissioning guidance within the UK and is an industry focus. Newer installations have undergone life cycle analysis as part of their design phase, but previously, this was not considered with older installations (Milios et al., 2019). Ways to decommission an installation safely and sustainably need to be developed but there is lack of communication and knowledge sharing between stakeholders and subcontractors (Wilkinson et al 2016), (Dagbui 2017). There is also a lack of data with regards to decommissioning and the handling of hazardous materials (Tan et al 2021).

## 2. Aims & Objectives

This conference paper aims to further the understanding of the handling of decommissioning hazardous waste materials utilising a bayesian network (BN) to analyse the interactions between the factors that affect the handling of these materials.

The aim will be met through the following objectives:

 i. The creation of a Bayesian network is based on previous research conducted by the author (Ford et al, 2023).

 ii. Analysis of the Bayesian network through a series of test cases.

## 3. Novelty

The novelty of this research project lies in the fact that despite decommissioning being a significant issue in the offshore oil and gas industry, there has been no research specifically on the handling of hazardous waste materials.

## 4. Methodology

This research paper forms part of a larger research project being undertaken at Liverpool John Moores University. The initial stage of the research involved a literature review to identify the current issues within the decommissioning process and identify if any, gaps in the regulatory framework. The findings of the literature review (Ford et al, 2021) were then used to inform an analytical hierarchy process and the development of a Bayesian Network.

Bayesian networks can be used to explore relationships between key factors and find outcomes for a system in a straightforward, visual manner. Bayesian networks are a type of directed acyclic graph that uses Bayes' Theorem (Neapolitan, 2004). They are constructed using nodes and links where the nodes represent variables which can either be discrete or continuous. The links between the nodes indicate causality.

## 5. Data Acquisition & Analysis

The focus of the model was to determine the interaction between the critical factors identified through expert discussions and AHP analysis completed as previous research by the author (Ford et al, 2023). The BN consists of 12 nodes, the data for which comes from a variety of sources. The numerical data has been obtained from a combination of these analyses and publicly available data from the HSE and OPRED close-out reports. If no decommissioning activities are taking place, then no further action is required. If decommissioning is taking place, is there a complete materials and equipment inventory available, and has a full survey of materials and equipment taken place? If the materials have been identified, have the correct permits for transport been applied for? If not, the consequence would be a liability event. Nodes seven and eight are concerned with whether the decontamination of hazardous waste equipment would take place offshore whilst on the installation or onshore after the equipment has been transported.

In the event that decontamination occurs offshore, the hazardous waste would be transported in tote tanks to an onshore site. If decontamination is to take place onshore, it is assumed that the equipment concerned would be isolated for transport. In the event of any failure or leak during transport, the consequence would be an environmental event. The final destination of hazardous waste is either recycling, reusing, or landfilling. The data for this node has been compiled from the publicly available close-out reports for completed decommissioning projects. The finalised model is shown in figure 1.

The model was validated using a sensitivity analysis and a series of test cases. The sensitivity analysis was conducted using the sensitivity wizard in the Hugin software. The sensitivity analysis determines how responsive the model's output is to variations to the input values. This demonstrates that the model is working correctly.
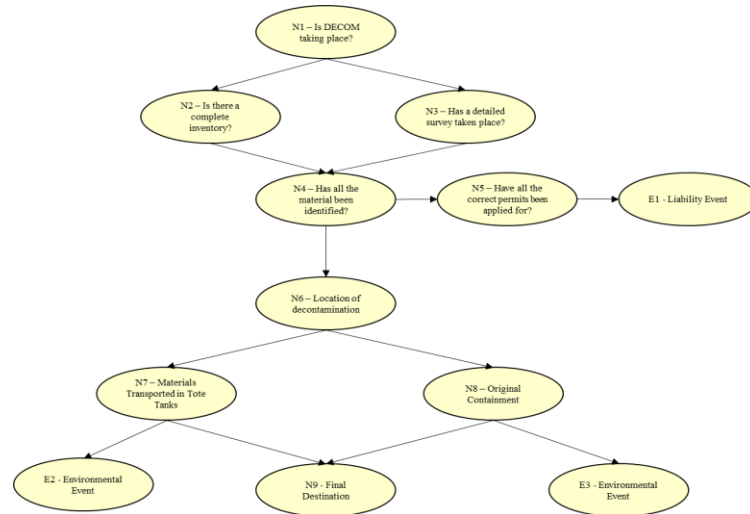


Figure 1 – Finalised bayesian network.

## 6. Results & Discussion

The marginalised probabilities for each node are shown in figure 2. Three different test cases were analysed to determine the influence of different parent nodes on a chosen child node.
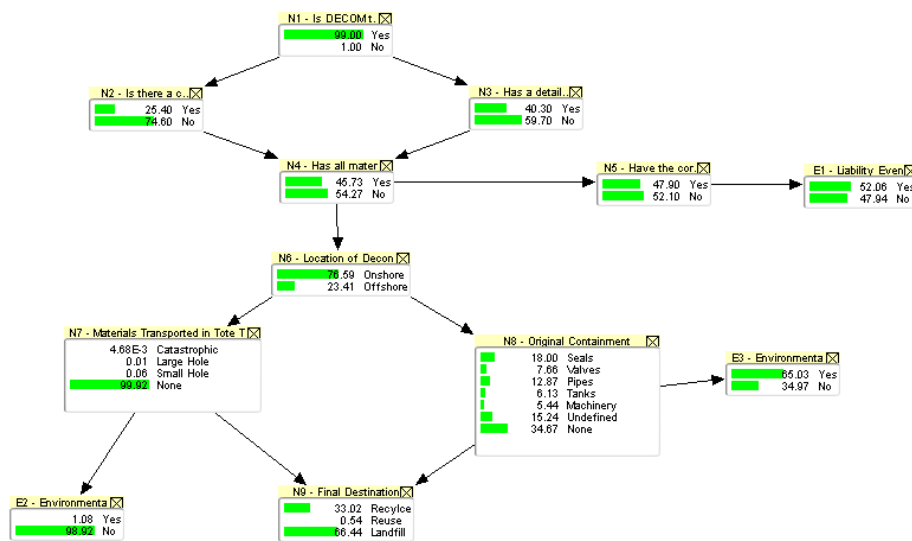


Figure 2 – Marginalised probabilities for the bayesian network.

Three different test cases were analysed to determine the influence of different parent nodes on a chosen child node. Test case 1 involved the scenario where nodes N2, N3 and N4 were in a state of 100% No. In this event, the probability of waste reaching landfills increases from 66% to 71%, and the possibility of waste materials being recycled decreases from 33% to 29%. This shows that in the event there is no comprehensive inventory present, and no detailed survey has taken place, the probability of the waste materials being correctly identified decreases, and more waste would be destined for landfill. This would reduce the sustainability of the overall decommissioning project, increase the risk of mishandling, and lead to further consequences.

Test case 2 involved the scenario where nodes N2, N3, and N4 are in a state where 100% Yes. In this scenario, all the historical information concerning equipment and materials is present, the surveys have been completed to a high standard, and the waste materials present have been correctly identified. This resulted in an increase in the probability of the waste materials being recycled or reused, ultimately increasing the sustainability of the overall project.

Test case 3 focused on the failure of containment during transport. Node 7 is set to 100% catastrophic failure of tote tanks. The effect on the final destination node was an increase in probability of the waste materials reaching landfill of 66.4% to 99.8%.

## 7. Conclusion

The Bayesian network shows that the final destination of hazardous waste materials is ultimately influenced by their identification. This is dependent on the historical information available and the quality of the survey and testing during the initial decommissioning process. It follows that if hazardous waste materials are incorrectly identified or their presence unknown, they may eventually end up in landfill instead of recycling or reuse. It also increases the risk of environmental or personnel accidents when the material reaches the onshore processing site.

In conjunction with the findings of the previous research, which highlighted the issues surrounding the understanding of legislation, lack of knowledge sharing and the emphasis on reducing costs, this highlights the current issues with decommissioning occurring in the UKCS. Despite stringent legislation and regulations, there is still uncertainty in their understanding.

## 8. Further Work

The results from the Bayesian network, alongside the findings of the previous paper, will be used to develop a holistic decommissioning framework that focuses on the handling of hazardous waste materials. This will be used by stakeholders in the decommissioning process as guidance alongside the current legislation and regulations.

## 9. References

Anderson, G., Rowles, B., Supple, S., Phillips, C. and Sühring, R. (2018) Comparison of substitution status of chemical substances under REACH and OSPAR legislation. Environmental Impact Assessment Review, 72, 43-49.

Brady, S. (2022) Practice Notes: Offshore Installations: Environmental Compliance and Pollution Liabilities [online] Available at: https://ca.practicallaw.thomsonreuters.com/Document/I8abc652c1c9a11e38578f7ccc38dcbee/View/FullText.html?ppcid=0c37c01cbf3d46299675a624e0f19ff9&originationContext=knowHow&transitionType=KnowHowItem&contextData=%28sc.RelatedInfo%29 [Accessed: 01/01/2022]

Calder, J. "HSE: Planning for Success," in Offshore Deccommissioning Conference, St Andrews, Scotland, 2019. B. Das, "Generating Conditional Probabilities for Bayesian Networks: Easing the Knowledge Acquisition Problem," ed, 2008.

EU, "Directive 2008/98/EC (Waste Framework Directive)," Official Journal of the European Union, no. L312/3, 2008.

Ford, J., Loughney, S. Blanco-Davies, E., Shahroki, A., Armada Bras, A. and Wang, J., (2021) Benchmarking and Compliance in the UK Offshore Decommissioning Hazardous Waste Stream. Research Publishing Services, 2021.

Ford, J., Loughney, S., Blanco-Davies, E., Shahroki, A., Armada Bras, A. and Wang, J. (2023) Identification of Key Factors in the Decommissioning of Offshore Oil and Gas Installations. In: M. Brito, T. Aven, P. Baraldi, M. Čepin and E. Zio, eds., Proceedings of the The 33rd European Safety and Reliability Conference (ESREL 2023). Singapore: Research Publishing, p.609.

La Védrine, M.A.G., Sheahan, D.A., Gioia, R., Rowles, B., Kroeger, S., Phillips, C. and Kirby, M.F. (2015) Substitution of hazardous offshore chemicals in UK waters: an evaluation of their use and discharge from 2000 to 2012. Journal of Cleaner Production, 87, 675-682.

Loughney S, Wang J. Bayesian network modelling of an offshore electrical generation system for applications within an asset integrity case for normally unattended offshore installations. Proceedings of the Institution of Mechanical Engineers, Part M: Journal of Engineering for the Maritime Environment. 2018;232(4):402-420. doi:10.1177/1475090217704787

Matellini DB, Wall AD, Jenkinson ID, et al. Modelling dwelling fire development and occupancy escape using Bayesian network. *Reliab Eng Syst Safe* 2013; 114: 75–91.

Milios, L., Beqiri, B., Whalen, K.A. and Jelonek, S.H. (2019) Sailing towards a circular economy: Conditions for increased reuse and remanufacturing in the Scandinavian maritime sector. Journal of Cleaner Production, 225, 227-235.

Neapolitan, R.E., 2004. Learning bayesian networks (Vol. 38). Upper Saddle River: Pearson Prentice Hall.

NSTA (2022) North Sea Transition Authority - Overview 2022. London, UK: NSTA.

OEUK, "Decommissioning Insight 2022," ed. UK: The UK Offshore Energies Association Limited, 2022.

OGUK (2015) Guidelines on Late-Life Decommissioning Inspection and Maintenance – Issue 1. UK.

OSPAR (2010) The North-East Atlantic Environment Strategy. Strategy of the OSPAR Commission for the Protection of the Marine Environment of the North-East Atlantic 2010–2020. London, United Kingdom: OSPAR.

Parente, V., Ferreira, D., Moutinho dos Santos, E. and Luczynski, E. (2006) Offshore decommissioning issues: Deductibility and transferability. Energy Policy, 34 (15), 1992-2001.

Perks, D., Oil & Gas 2012 (Oil & Gas 2012). Sweet & Maxwell, 2012.

Sühring, R., Cousins, A., Gregory, L., Moran, C., Papachlimitzou, A., Phillips, C., Rowles, R., Supple, S., Wilczynska, M. and Birchenough, S.N.R. (2019) The past, present, and future of the regulation of offshore chemicals in the North Sea—a United Kingdom perspective. ICES Journal of Marine Science, 77 (3), 1157-1166.

Weber, P. and Simon, C., 2016. Benefits of Bayesian network models. John Wiley & Sons.

# Zeyu Hu
# Postgraduate Researcher
# School of Engineering

# Impact of Rs on Switching Process and 1S1R operation with GeAsTe Ovonic Threshold Switching (OTS) Selectors

Zeyu Hu[1], Weidong Zhang[1], Robin Degraeve[2], Daniele Garbin[2], Zheng Chai[3], Nishant Saxena[1], Pedro Freitas[1], Andrea Fantini[2], Taras Ravsher[2], Sergiu Clima[2], Jian Fu Zhang[1]

[1] School of Engineering, Liverpool John Moores University, Liverpool, United Kingdom
[2] IMEC, 3001 Leuven, Belgium
[3] School of Materials Science and Engineering, Xi'an Jiaotong University, Xi'an, China

E-mail address: Z.Hu@2020.ljmu.ac.uk

**Abstract.** Experimental evidence and analysis in this paper provide new insights into the fast-switching process in GeAsTe ovonic threshold switching (OTS) selectors. The full switching-off process, covering the defect cluster shrinking and rupture, can be measured and characterized. Two distinct switch-off mechanisms and their dependence on the total impedance of 1S1Rs are identified. The impact of Rs value on the switching process and its underlying mechanism can be explained by the dynamic resistance of OTS induced by the transition of defect clusters.

**Keywords.** Ovonic Threshold Switching, Selector, emerging memory, 1S1R

## 1. Introduction

Selector device plays a key role in suppressing the sneak path currents in the crossbar arrays that utilize the emerging non-volatile memory devices [1], such as the phase change memory (PCRAM), and resistive switching memory (ReRAM). The selector is required to have fast volatile switching characteristics and is connected in series with the non-volatile memory device. When the memory device is not selected, it is biased at a half of the operation voltage, at which the selector should have very low off-state current and can suppress the overall leakage current. When the memory device is selected at the operation voltage, the selector is at the ON state, and should allow a sufficiently high current to pass through so that the memory device can be programmed.

Therefore, a large on-off current ratio is an essential requirement for the selector [2]. Among the many different types of selector devices, the ovonic threshold switching OTS in chalcogenide materials such as GeSe and GeAsTe [3], is a promising candidate. It has many virtues such as fast switching speed in the order of ns, high ON-state current density larger than 20MA/cm$^2$, high half-bias nonlinearity larger than $10^5$, and excellent endurance more than $10^{12}$ cycles [4].

The switching process in OTS has been described by different models, including the earlier thermally induced instability model, the electronic injection induced space charge model, and more recently, the electric field induced local bond modification models. In the latest models [5], the defects transition from the ground state to the excited state at a high field due to the local bonds modification and become delocalized, so that the defect clusters are formed which led to the off-to-on switching, and vice-versa.

Furthermore, the operation of 1S1R in which the selector is connected with a series resistor (Rs) were also investigated, and it was suggested that the Rs plays an important role in the switching-on and switching-off process [6]. For example, it was found that Rs defines the load line for the selector and hence its operation points and the holding current, so that the selector is either switching volatilely

between the static off-state and on-state, or oscillating in the transitional negative-differential-resistance (NDR) [7]. Despite these early efforts, detailed experimental evidence is still lacking for characterizing the fast and sharp switching process in modern OTS devices. For example, it is not clear how the switching process and parameters in nanoscale OTS devices are affected by the series resistance and what are the corresponding OTS switching mechanisms, which should provide important information for understanding the operation and modelling of the 1S1R circuit.

In this paper, based on novel analysis, we observed the full OTS switching-off process and two distinct mechanisms of OTS switch-off. The defect cluster shrinking kinetics is Rs independent after the normalization, but its rupture is dependent on Rs. Also we investigated on the impact of Rs on 1S1Rs operations and parameters.

## 2. Device and measurement

A 20nm amorphous GeAsTe chalcogenide film is deposited by room temperature physical vapor deposition (PVD) and passivated with a low-temperature BEOL process. The TiN/GeAsTe/TiN selector uses a pillar (TiN) bottom electrode that defines the device size down to 50 nm and integrates with a serial resistor Rs in the range of 1.8 kΩ to 400 kΩ in a 300 mm process flow (**Fig.1a**). A triangle pulse is used to record the bias and current during the AC switching (**Fig.1b**).
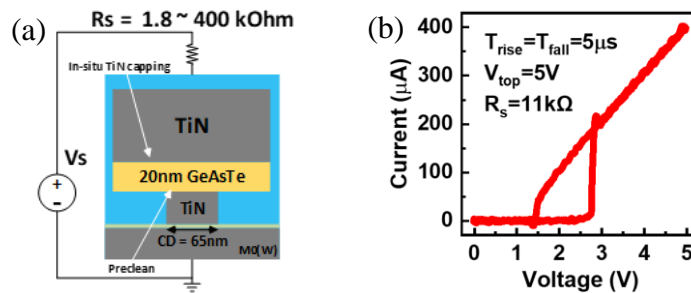


Fig. 1 (a) Illustration of the OTS structure in series with a resistor Rs. (b) A typical I-V of 1S1Rs measured by a triangular pulse. Pulse conditions and Rs value are labelled.

The I-V characterization was carried out by using a Keithley 4200A semiconductor analyser either with the SMU for DC sweep or with the embedded 4225-PMU ultrafast I-V module for voltage sweep.

## 3. Results and discussion

### 3.1 New observation in OTS-only I-V with different Rs

OTS-only I-V can be obtained from the overall 1S1Rs I-V by subtraction, $V_{OTS} = V_{1S1R} - I \cdot R_s$, as the linear I-V at ON-state is dominated by Rs. However, when Rs≥80 kΩ, a significant non-linear ON state (NL-ON) region is observed, before OTS switches to OFF state (**Fig.2a**). The results of DC V-sweep, DC I-sweep and pulse switching are compared (**Fig.2b&c**), and the NL-ON region is observed and overlaps in all three cases when Rs≥80kΩ, confirming that it is not caused by the test method or test speed, or RC effects in the setup.
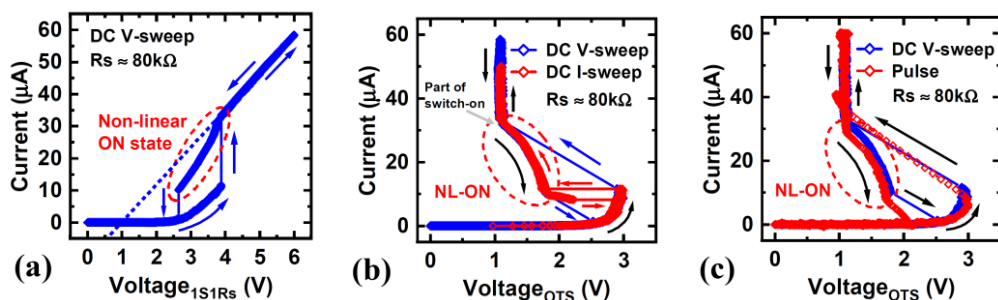
Fig.2 (a) a significant non-linear ON state region is observed before OTS switch to OFF state with Rs≈80 kΩ. (b) Both DC V-sweep and I-sweep show NL-ON that overlap with each other during switch-off. (c) Good agreement is observed in DC and pulse V-sweep, supports that NL-ON is a true phenomenon.

In contrast, when Rs≤30 kΩ, a much subtler NL-ON is observed, in which V-sweep also overlaps with I-sweep (**Fig.3a**) and pulse switching (**Fig.3b**). The agreement of UP & Down traces in NL-ON of both sweeps suggests that it is a common feature for both switch-on and -off processes.
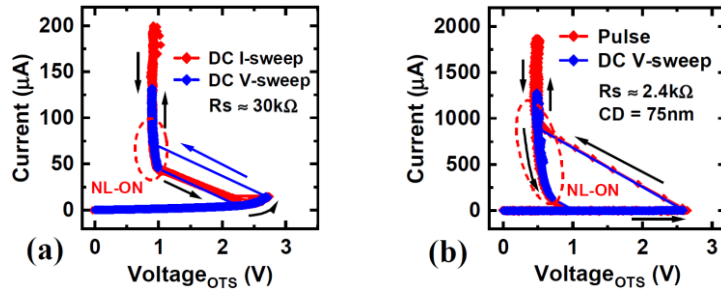


Fig.3 (a) a subtle NL-ON region is observed when Rs≤30 kΩ in both DC V-sweep and I-sweep for example. (b) Good agreement is also observed in DC and pulse V-sweep.

*3.2 Characterisation of switch-off process*

To understand the mechanism of the NL-ON region, the gradient $R_{diff} =dV/dI$ is defined as the dynamic resistance of OTS-only (Fig.8a&b), which is near zero at linear ON state. The I-V curves enter the NL-ON at ($I_{hold\_OTS}$, $V_{hold\_OTS}$), where the |Rdiff| increases, due to defect clusters shrinking with decreasing current, is no longer negligible in comparison to Rs. OTS switches off at ($I_{hold\_off}$, $V_{hold\_off}$) when the defect clusters rupture, at the OTS holding point commonly used for 1S1R [8-9], where $R_{diff}=R_{diff\_off}$. The switching-off process is clearly different for Rs≤30 kΩ and Rs≥80 kΩ, indicating it is controlled by two different mechanisms. For smaller Rs, OTS switches off when |Rdiff_off| reaches Rs (≤30 kΩ) where the total impedance of the 1S1Rs circuit, Rs+Rdiff, becomes 0 (**Fig.4a**). For larger Rs, the maximum value of |Rdiff|, |Rdiff_max|, can no longer reach Rs (80kΩ-400kΩ), hence the total impedance of 1S1Rs remains positive. OTS current must decrease to a minimum holding level to trigger the switch-off (**Figs.4b**).
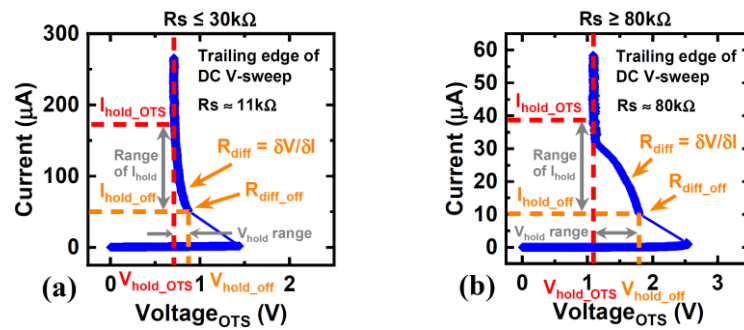


Fig.4 Definition of $V_{hold\_OTS}$, $I_{hold\_OTS}$, $V_{hold\_off}$ and $I_{hold\_off}$ for OTS-only (a) when Rs≤30kΩ, and (b) when Rs≥80kΩ.

The above analysis agrees in principle with the previous defect clusters model for OTS with a field and current dependent transition dynamics [5]. When OTS current reduces, the defect clusters shrink, and the defect number in the clusters reduces, so that |$R_{diff}$| increases and $V_{OTS}$ increases. When |Rdiff| reaches the Rs (≤30kΩ), the total impedance of 1S1Rs becomes 0 and the OTS is out of equilibrium and switches OFF at $V_{hold\_off}$. For larger Rs (≥80kΩ), |$R_{diff\_max}$| can no longer reach Rs, OTS is forced to operate at NL-ON state in a low current regime, where $I_{OTS}$ keeps decreasing until it is below the minimum OTS holding current, then the conductive cluster is broken and OTS switches OFF.

*3.3 Impact of Rs on 1S1R operations*

The NL-ON will lead to large errors when reading the memory element of large R values (**Fig.2a**). It is also found that both the $V_{th\_OTS}$ and $V_{hold\_OTS}$ increase with Rs values, due to the weaker defect clusters because of smaller OTS operation currents (**Fig.5b**). Hence the OTS-only $V_{th}$ and $V_{hold}$ also contribute to the total $\Delta V_{th}$ & $\Delta V_{hold}$ in 1S1R operation, in addition to that caused by the programmable R value. Both these Rs dependence of $I_{hold\_off}$ and $V_{th\_OTS}/V_{hold\_OTS}$ (**Fig.5a**) should be accounted for in the 1S1R circuit simulation and analysis.
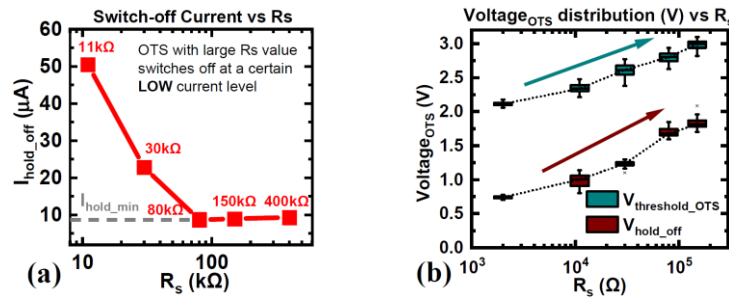


Fig.5 (a) $I_{hold\_off}$ and (b) $V_{hold\_off}$ vs Rs for OTS-only.

**4. Conclusion**

Experimental evidence are provided in this paper to reveal the full switch-off process of GeAsTe OTS, in which the OTS switches off at $R_{diff\_OTS}+Rs=0$ when $Rs<|R_{diff\_max}|$, but at the $I_{hold\_min}$ when $Rs>|R_{diff\_max}|$. The resulted non-linear ON region has significant impact on the parameters and simulation of 1S1R operation.

**Reference**:

[1] G. Burr, R. Shenoy, et al, Journal of Vacuum Science & Technology B, vol. 32, no. 4, p. 040802, 2014.

[2] S. Jia, H. Li, et al, Nat Commun, vol. 11, no. 1, p. 4636, Sep 15 2020, doi: 10.1038/s41467-020-18382-z.

[3] Z. Chai, P. Freitas, et al, IEEE Electron Device Letters, vol. 41, no. 10, pp. 1496-1499, Oct 2020, doi: 10.1109/Led.2020.3017095.

[4] Y. Koo, K. Baek, and H. Hwang, 2016 IEEE Symposium on VLSI Technology, 2016: IEEE, pp. 1-2, doi: 10.1109/VLSIT.2016.7573389.

[5] R. Degraeve, T. Ravsher S. Kabuyanagi, et al, 2021 IEEE International Reliability Physics Symposium (IRPS), 2021: IEEE, pp. 1-5.

[6] J. M. Lopez, N. Castellani, et al, 2021 IEEE Int. Memory Workshop (IMW), 2021: IEEE, pp. 1-4, doi: 10.1109/IMW51353.2021.9439606.

[7] R. Pryor and H. Henisch, Journal of Non-Crystalline Solids, vol. 7, no. 2, pp. 181-191, 1972, doi: 10.1016/0022-3093(72)90288-8.

[8] Cheng, H. Y., et al, 2018 IEEE International Electron Devices Meeting (IEDM). IEEE, 2018.

[9] Chai, Z., et al, 2019 Symposium on VLSI Technology. IEEE, 2019.

# David Law
# Postgraduate Researcher
# Astrophysics Research Institute

# Using Deep Q-network Based Deep Reinforcement Learning for the Automated Scheduling of Astronomical Observations

David J Law

Institute Address: Astrophysics Research Institute, Liverpool John Moores University

E-mail address: d.j.law@2021.ljmu.ac.uk

## Abstract

As time-domain astronomy progresses, the necessity for efficient and intelligent scheduling of astronomical observations intensifies. This study introduces a novel application of Deep Q-Network (DQN) based Deep Reinforcement Learning to address the dynamic scheduling challenge posed by transient astronomical phenomena. A DQN agent was devised and trained to emulate the Liverpool Telescope (LT) scheduling behaviour, focusing on factors such as task priority and environmental seeing conditions. The simulation-based training environment and the finely-tuned reward system underpin the agent's ability to prioritise observations, successfully emulating the LT's scheduling strategy. The agent's performance demonstrates promising potential for real-time, adaptive decision-making within operational telescopes. This research sets the baseline for future advancements in reinforcement learning within astronomical scheduling, suggesting that DQN-based models could significantly contribute to the intricacies of telescope scheduling, improving observational efficiency and increasing scientific output.

**Keywords:** Telescope scheduling, Deep reinforcement learning, Decision-making automation, Dynamic scheduling, Simulation, Agents, Deep Q-network.

## 1. Introduction

In the dynamic field of time domain astronomy, swift and efficient observation of changing celestial phenomena, from supernovae to variable stars, is crucial. The introduction of the New Robotic Telescope (NRT), which succeeds the two-decade-long contributions of the Liverpool Telescope (LT), calls for a scheduling system that matches its advanced capabilities for rapid and intelligent decision-making. Traditional rule-based systems fall short in maximising the NRT's potential, particularly for observing transient events that are both fast and faint. This paper introduces a pioneering Deep Q-Network (DQN)-based Deep Reinforcement Learning (DRL) strategy tailored for the NRT's scheduling challenges. By mimicking the LT's scheduling, this method aims to set the foundation for enhancing the NRT's decision-making efficiency and scientific yield and for future advancements in astronomical scheduling. It explores the DQN-based DRL's theoretical basis, methodological execution, and implications for evolving the precision and responsiveness of time-domain astronomical observation.

## 2. Background

### 2.1 Decision Making in Dynamic Environments

The scheduling of astronomical observations is an example of a dynamic scheduling problem, where the schedule is processed simultaneously as new jobs are coming into the queue, or the constraints driving the decision-making are subject to change [1]. While sufficient for static or mildly dynamic settings, traditional heuristic or deterministic algorithms falter under the unpredictable changes typical of time-domain astronomy. The Liverpool Telescope (LT) addressed this with a myopic dispatch scheduler that dynamically re-prioritises targets, albeit at the expense of long-term planning efficiency.

Markov Decision Processes (MDP) offer a sophisticated approach to address these scheduling challenges by creating a unified model that captures the stochastic nature of the environment. This model is defined through states, actions, and the transitions between them, accompanied by rewards for each transition [2, 3]. A key feature of MDPs is the Markov property; the likelihood of transitioning to

future states depends solely on the present state, not the preceding events. This property ensures that all necessary information for future decisions is contained within the current state representation [4]. Using MDPs as a foundational framework, we can apply advanced reinforcement learning techniques, such as Deep Q-Networks (DQN), to emulate and improve the LT's scheduling strategy. DQNs offer a dynamic and comprehensive decision-making tool, making them well-suited for adapting to the complexities of astronomical scheduling.

## 2.2 Reinforcement Learning

Reinforcement learning (RL) is an agent-based machine learning (ML) method where agents learn to take actions within a given environment and are rewarded for suitable actions to maximise the reward generated. This reward shapes future actions as shown in figure 1. An RL algorithm, however, operates with limited knowledge of the situation and relatively limited feedback on the quality of the decisions made [5].



Figure 1: The Reinforcement Learning Loop.

## 2.3 Deep Q-Networks (DQN)

Historically, a significant challenge for RL techniques was processing high dimensional data [6]. This dimensionality presents a particular challenge in dynamic scheduling problems, such as scheduling astronomical observations. With Q learning, the Bellman Equation optimises the dynamic decision-making process, such that the reward for a given state action pair $Q^{\pi}(x, a)$ s a combination of the reward for a given action $R_x(a)$ and the sum of the rewards for future actions $\sum_y P_{xy}[\pi(x)]V^{\pi}(y)$ given the policy $\pi$ adjusted by a discount factor $\gamma$ [7].

$$Q^{\pi}(x, a) = R_x(a) + \gamma \sum_y P_{xy}[\pi(x)]V^{\pi}(y). \tag{1}$$

For high dimensional data, the action-value function $Q^{\pi}(x, a)$ becomes computationally intractable as this needs to be calculated separately for each sequence. A deep neural network model DNN is used instead to estimate the Q values by querying the output nodes of the network; instead of making updates to individual Q values, the updates in the learning process are made to the parameters of the network [6, 8]. This shift into a deep learning-based approach means that it is possible for a DQN to effectively process the full range of observational data and constraints, making DQN-based real-time decision-making a potential solution to the telescope scheduling problem.

## 2.4 Towards a Practical Framework

The advent of DQN-based decision-making in astronomical scheduling marks a significant transition from heuristic-driven, rule-based systems to a data-centric, intelligent framework. The application of a DQN-based DRL agent is set to revolutionise this process by allowing the computational power of neural networks to process complex, high-dimensional data adaptively. This development promises enhancements in real-time decision-making for telescope scheduling within the transient follow-up domain,

which will be explored through the subsequent methodology. The focus will be on the reward system's intricacies and the DRL agent's overall efficacy in replicating the behaviour of the LT scheduler.

## 3. Methodology

### 3.1 Agent and Model Architecture

A deep Q-network agent was implemented using PyTorch (1.13.1) [9]. The model consisted of three fully connected layers. The first two layers, followed by a ReLU activation function, transformed the input state into a 64-dimensional feature space. The ReLU activation was chosen to mitigate the potential vanishing gradient problem with computational efficiency [10]. The third layer mapped these features to action values corresponding to each possible action. The observational parameters and the number of observations within the training simulation determined the state size, and the action size was set based on the potential targets available at any scheduling step. The choice was made initially to keep the architecture of the network relatively small, which proved sufficient for replicating the behaviour of the relatively simple LT scheduler.

### 3.2 State, Action, and Reward Definition

The state representation included normalised time, the ratio between a target's maximum and current altitude, encoded priority, seeing match score, urgency flag, and timing constraint type for each potential target, resulting in a comprehensive view of the scheduling scenario at each timestep. Actions were defined as selecting a target to observe, with rewards structured to prioritise observations based on scientific value, urgency, and the match between current seeing conditions and target constraints.

### 3.3 Simulation Environment

A custom simulation environment was developed to mimic the operational and observational conditions of the Liverpool Telescope. This environment provided a framework for training the DQN agent by simulating the decision-making process for scheduling astronomical observations. The simulation included models for target visibility, sky conditions, and telescope operational status, enabling a realistic approximation of the scheduling challenges.

### 3.4 Training Process

The agent trained using a simulation environment for a pre-defined count of 1400 episodes, a decision informed by preliminary experiments to optimise the balance between learning efficiency and model generalisation. At each timestep, the agent executed actions based on an epsilon-greedy policy, facilitating a strategic balance between exploring new actions and exploiting known strategies. The accumulation of experiences in a replay buffer and subsequent sampling for model updates through backpropagation was pivotal in minimising the mean squared error between predicted and target Q-values, thereby refining the agent's decision-making capabilities.

### 3.5 Implementation Details and evaluation

The model utilised the Adam Optimiser [11] with an initial learning rate of 0.001, adjusting it through a learning rate schedule for ongoing improvement. An epsilon-greedy policy, starting with epsilon at 1.0 and decaying over time, facilitated the transition from exploration to exploitation. After training, culminating in a final loss value of 0.86, the agent underwent rigorous evaluation against the LT scheduling algorithm by comparing the DQN output to an established benchmark.

## 4. Results

The developed DQN agent was evaluated for its ability to replicate the decision-making process of the Liverpool Telescope's scheduling system. The assessment focused on the agent's performance in reproducing the decision-making of the LT algorithm. This evaluation focused on all of the decision-making constraints of the LT algorithm: elevation as a function of its maximum elevation, priority rank, urgent flag, timing constraint type, and seeing matching score. Although only two are presented here, priority and seeing matching.

### 4.1  Priority-Based Decision-Making

The agent's fidelity to the LT's priority-based scheduling was analysed by varying the priority of tasks while controlling for other variables. Figure 2 illustrates the model's capacity to prioritise tasks over time. The plot reveals that the agent consistently chose higher-priority tasks, which is aligned with the LT's scheduling policy.
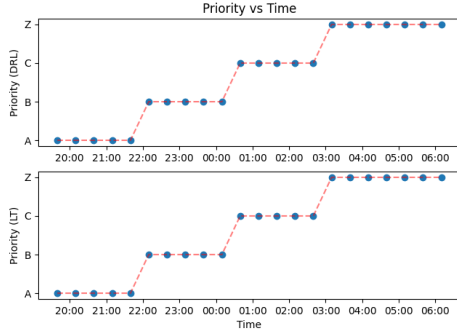


Figure 2: Priority-based target selection over time, demonstrating the agent's consistent adherence to the hierarchical importance of observational tasks.
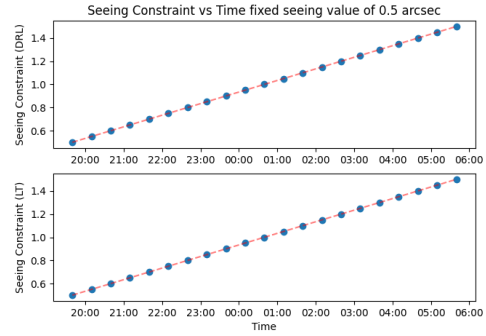


Figure 3: The agent's decision adjustment corresponds to the variation in seeing constraints, reflecting its proficiency in optimising observational quality under dynamic environmental conditions.

### 4.2  Seeing matching

The agent's ability to correctly prioritise seeing was assessed by fixing the seeing value in the simulation and providing data where the seeing constraint varied by 0.05 with each group. As depicted in figure 3, the agent can correctly select targets where the seeing constraint more closely matches the seeing conditions, mimicking the LT's seeing-matching strategy effectively.

## 5.  Discussion and Future Work

The results from the DQN agent successfully emulate the LT scheduler, showing the potential of reinforcement learning in astronomical scheduling. This demonstrates the agent's ability to prioritise based on multiple factors, including constraints and urgency, making it valuable for adaptive, real-time decision-making. Notably, its responsiveness to dynamic conditions has the potential to improve efficiency, which is vital for time-sensitive astronomical targets. However, the DQN's performance in a more comprehensive and unpredictable operational context remains to be fully explored.

The study also highlights the importance of an accurately designed reward system in guiding the learning process towards the desired outcomes. Fine-tuning the reward function emerged as a decisive factor in the agent's ability to emulate decision-making within the LT scheduler.

There are several avenues for expanding upon this research. An immediate direction is enhancing state representations to include additional parameters, such as the slew distance, which could offer more granular control and improve the scheduler's efficiency. Further research could also involve integrating less well-defined science cases, challenging the DQN to perform under more varied conditions. This challenge includes adapting the system for upcoming programmes like the SPEC Survey for NRT.

Additionally, an in-depth exploration of the DQN's parameter space could uncover new insights into the balance between exploration and exploitation, potentially leading to even more efficient scheduling strategies. As artificial intelligence becomes increasingly intertwined with astronomical research, developing robust, versatile, and adaptive scheduling agents will be imperative. This study serves as a stepping stone towards realising the potential of DRL in this domain.

# References

[1] M. Mora and M. Solar, "A Survey on the Dynamic Scheduling Problem in Astronomical Observations," in *Artificial Intelligence in Theory and Practice III*, M. Bramer, Ed. Berlin, Heidelberg: Springer, 2010, pp. 111–120.

[2] S. N. Fraser, "Adaptive Optimal Telescope Scheduling," Ph.D. dissertation, Liverpool John Moores University, 2012.

[3] R. Bellman, "A Markovian Decision Process," *Journal of Mathematics and Mechanics*, vol. 6, no. 5, pp. 679–684, 1957.

[4] M. van Otterlo and M. Wiering, "Reinforcement Learning and Markov Decision Processes," in *Reinforcement Learning: State-of-the-Art*, M. Wiering and M. van Otterlo, Eds. Berlin, Heidelberg: Springer, 2012, pp. 3–42.

[5] C. Shyalika, T. Silva, and A. Karunananda, "Reinforcement Learning in Dynamic Task Scheduling: A Review," *SN Computer Science*, vol. 1, no. 6, p. 306, Sep. 2020.

[6] V. Mnih, K. Kavukcuoglu, D. Silver, A. Graves, I. Antonoglou, D. Wierstra, and M. Riedmiller, "Playing Atari with Deep Reinforcement Learning."

[7] C. J. C. H. Watkins and P. Dayan, "Q-learning," *Machine Learning*, vol. 8, no. 3, pp. 279–292, May 1992.

[8] M. Hausknecht and P. Stone, "Deep Recurrent Q-Learning for Partially Observable MDPs," Jan. 2017.

[9] A. Paszke, S. Gross, F. Massa, A. Lerer, J. Bradbury, G. Chanan, T. Killeen, Z. Lin, N. Gimelshein, L. Antiga, A. Desmaison, A. Köpf, E. Yang, Z. DeVito, M. Raison, A. Tejani, S. Chilamkurthy, B. Steiner, L. Fang, J. Bai, and S. Chintala, "PyTorch: An Imperative Style, High-Performance Deep Learning Library," Dec. 2019.

[10] A. F. Agarap, "Deep Learning using Rectified Linear Units (ReLU)," Feb. 2019.

[11] D. P. Kingma and J. Ba, "Adam: A Method for Stochastic Optimization," Jan. 2017.

# Maisem Moammer
## Postgraduate Researcher
## School of Engineering

# Development of a readiness evaluation framework for transitioning conventional ports to smart ports.

**Moammer Maisem\* [a], Pyne Robyn [a,], Jin Wang [a], Dimitrios Paraskevadakis [a], Musa Bashir [a,]**

[a] Liverpool Logistics, Offshore and Marine Research Institute (LOOM), Liverpool John Moores University, Liverpool,

**Abstract:** The integration of intelligent technologies with physical port logistics has led to the emergence of smart ports. These ports leverage Information and Communication Technology (ICT) solutions to meet the demands of numerous vessels transporting substantial cargoes within shortest timeframes. Concurrently, smart ports aim to reduce the environmental consequences associated with port activities, such as energy consumption and carbon emissions. The aim of this investigation is to critically examine the state-of-the-art on smart ports development, with the view to developing a framework for converting traditional ports. The study uses the Port of Hamburg in Germany as a benchmark to understand the requirements of a smart port in relation to transitioning a traditional port to a smart port. The study examined the key aspects of smart port that are responsible for improving service efficiency, particularly in terms of time optimisation and energy savings. The analysis identifies key factors that influence the adoption of a smart port, based on both existing literature and the case study using expert judgement. Notably, the study highlights that port infrastructure stand as the key influential factor in the implementation of a smart port. In addition, survey respondents identified other pivotal factors such as energy efficiency and environmental impact in the context of smart port deployment as contributory factors.

**Keywords:** Smart port. Port of Hamburg. infrastructure. Energy efficiency. Environmental impacts.

## 1. Introduction

Port operators are increasingly seeking for solutions to optimise port operations, improve efficiency, and reduce logistics costs. Achieving these goals depends on the integration of modern communication technologies based on internet of things (IoT), with traditional port operations. However. The technologies are aimed at expediting the handling of substantial cargo volumes that most ports have to deal with regularly. While the traditional practice of manual loading and unloading by dockside workers has gradually diminished, the unforeseen progression shows a scenario where vessels arrive at ports for immediate unloading without any visible human intervention. From this perspective, the increasing integration of SPs around the world maximizes port efficiency while minimizing energy use and increasing environmental protection using modern technology and Internet-based applications, enabling increased efficiency in logistical operations, and thus brining macroeconomic benefits to global and national trade. This research aims to develop a model that ports can use to conduct an assessment of readiness to implement SP projects, discovering the most important factors that affect the adoption of the SP project (Belmoukari, Audy, and Forget, 2023).

## 2. Literature review

### 2.1. Basic concept and characteristics of a Smart Port

SPs are considered synonymous with automated or robotic ports in some contexts but while these are intrinsic features of these ports, the SP concept goes far beyond. Although there is no uniform definition of SP, researchers agree that SPs are generally related to improving port productivity using advanced ICT and automated systems, integrating IoT and supply chain management, and increased attention to environmental friendliness (Rajabi et al., 2018). Traditional ports focus on the movement of ships and

goods by importers and exporters, connecting sea and land, and providing docking facilities for loading and unloading passengers and goods (Karaś, 2020). SPs have moved beyond this, collecting and managing data for the purpose of linking whole supply chains and technological innovations to increase port efficiency, while reducing pressure on the environment (Belmoukari, Audy, and Forget, 2023).

## 2.2 Example of SP implementation in Europe (Port of Hamburg)

The Port of Hamburg (hereinafter 'Hamburg') is the largest port in Germany and the third largest container port in Europe. Hamburg is one of the world's largest high-performance ports, dating back to the ninth century. The port has an area of 7200 hectares, and is located 110 km from the mouth of the river Elbe on the North Sea. It is considered the most import port handling goods in northern Europe, linking 178 countries worldwide. The Port provides about 133,000 jobs for the city of Hamburg and about 22,000 beneficiaries from neighboring areas, directly or indirectly. (Hamburg Port Authority, 2023).

## 3. Methodology and Methods

This research aims to develop a model that ports can use to conduct an assessment of readiness to implement SP projects. More specifically, the research focus is on:

1.Reviewing related literature in this field to identify critical issues in SP projects. 2. Developing a model that can be used to assess ports' readiness to implement SP. 3. Validating the model (by experts). 4. Testing a case study of a traditional port to test the model in a real situation.

### 3.1 Hierarchical decision model (HDM)

This study uses HDM as the research methodology, as conceptualized by Estep (2017). The model was developed by Kocaoglu and Cleland (1981) as a multi-criteria decision-making tool used in complex situations. HDM has different levels depending on the logical sequences and the complexity of the decision as well. The MOGSA hierarchy developed by Kocaoglu (1983) was used in this study. As depicted in Figure 1.
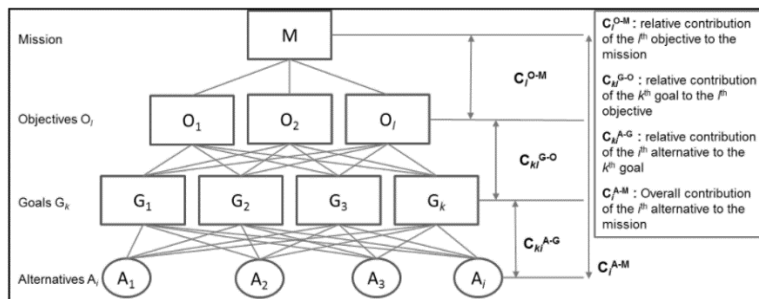


Figure 1. HDM design (Source: Estep, 2017).

### 3.2 Research framework
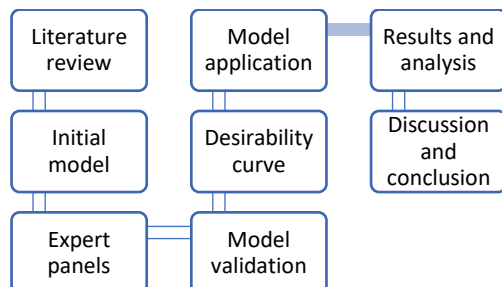
Figure 2 illustrates the research framework.



Figure 2. Research Framework

### 3.3 HDM Model

Based on the critical literature review, the HDM is structured with the main objective and four main perspectives. Moreover, each main perspective has several factors in order to assess the readiness of

traditional ports to implement SP projects. Experts were asked to validate each item. A total of 48 experts participated in the survey. Based on the expert's validation, figure3 illustrates the research model.
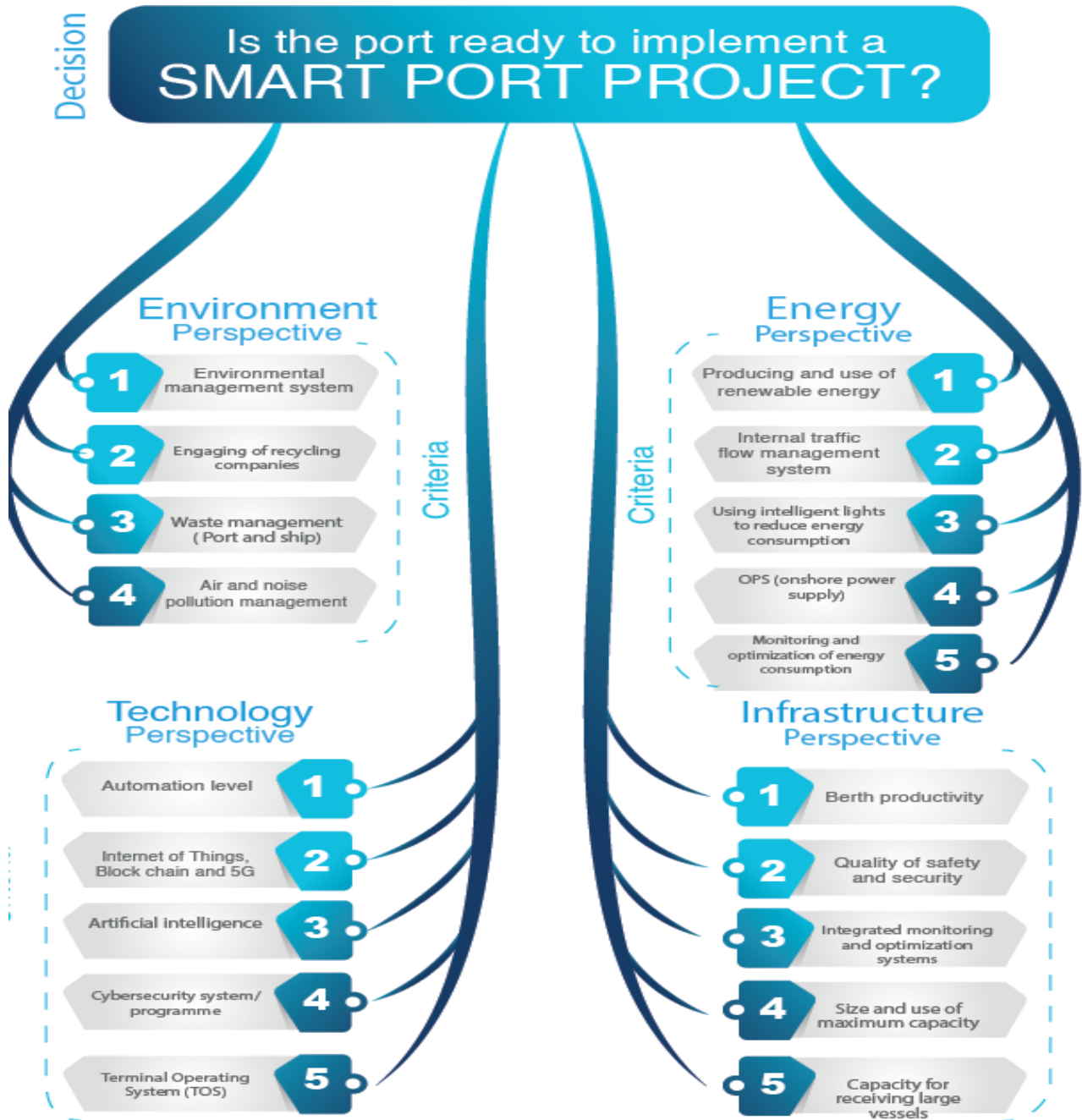


Figure 3 The Research Model

3.4 Quantification of the HDM Model

The stage that follows validation of the HDM model is the quantification stage, which involves ranking the factors based on their relative importance. Subjective judgments are expressed in pairwise comparisons, which are then converted into relative weights. At this stage, experts make pairwise comparisons in the hierarchical model (perspectives and factors) on a fixed sum measuring scale of 1-100 for each factor in the hierarchical model. Each factor has both a global and a local weight within its group. The factors were arranged, and the results were analyzed according to the following table.

Table 1 Overall model weight

| Perspective | Factors | Local Weight | Global Weight Local Weight *Perspective Weight |
|---|---|---|---|
| Energy (19.5%) | Producing and use of renewable energy | 31.7% | 6.20% |
| | Internal traffic flow management system | 18.9% | 3.70% |
| | Using intelligent lights to reduce energy consumption | 14.4% | 2.80% |
| | OPS (onshore power supply) | 14.5% | 2.82% |
| | Monitoring and optimization of energy consumption | 20.7% | 4.03% |
| Environmental (14.6%) | Environmental management systems | 39.8% | 5.81% |
| | Engaging of recycling companies | 14.9% | 2.2% |
| | Waste management (Port and ship) | 25.7% | 3.80% |
| | Air and noise pollution management | 19.7% | 2.90% |
| Infrastructure (36.3%) | Berth productivity | 23.2% | 8.42% |
| | Quality of safety and security | 29.5% | 10.70% |
| | Integrated monitoring and optimization systems | 17.5% | 6.40% |
| | Size and use of maximum capacity | 15.3% | 5.60% |
| | Capacity for receiving large vessels | 14.5% | 5.30% |
| Technology (29.5%) | Automation level | 25% | 7.40% |
| | Internet of Things, Block chain and 5G | 16.4% | 4.83% |
| | Artificial intelligence | 14% | 4.13% |
| | Cybersecurity system/ programme | 21.8% | 6.43% |
| | Terminal Operating System (TOS) | 21.4% | 6.31% |

## 5.Conclusion

In Smart Ports, many modern devices and sensors are connected to each other through the IoT. The Port of Hamburg was presented as a leading example of a SP, and this example proves that investing in SP projects that depend on IoT have proven to be successful. From this perspective and the importance of SPs, the author is looking into this field in order to implement this system in many ports around the world. The SP is a broad concept that encompasses many aspects related to port activities, yet there is limited interest from academic researchers. There is a need to identify the main factors affecting this area. This project is an attempt to find these factors.

In this article, the researcher carried out an assessment of the main factors that influence the implementation of a SP. This was conducted by first reviewing different literatures and previous studies on this subject, and establishing a common definition on the concept of SP. The author received 48 responses, The results were very interesting, revealing that port infrastructure is the most important main factor, followed by technology, and then energy and environmental.

## References

[1]. Belmoukari, B., Audy, J.F. and Forget, P., 2023. Smart port: a systematic literature review. European Transport Research Review, 15(1), pp.1-12.

[2]. Daim, T.U. and Kocaoglu, D.F. (2016) Hierarchical decision modelling: Essays in Honor of Dundar F. Kocaoglu. Berlin: Springer.

[3]. Estep, J. (2017) Development of a technology transfer score for evaluating research proposals: Case study of demand response technologies in the Pacific Northwest [online], Ph.D. dissertation, Portland State University DOI: 10.15760/etd.5363 [Accessed: 10th March 2022].

[4]. Hamburg Port Authority (2023). SMAR-T MAINTENANCE. [Online] Available at: https://www.hamburg-port-authority.de/en/hpa-360/smartport [Accessed: 13th of July 2023].

[5]. Karaś, A., 2020. Smart port as a key to the future development of modern ports. TransNav: International Journal on Marine Navigation and Safety of Sea Transportation, 14(1).

[6]. Kocaoglu, D.F. (1983) A participative approach to program evaluation. IEEE Transactions on Engineering Management, 3, pp.112-118.

[7]. Rajabi, A., Saryazdi, A.K., Belfkih, A. and Duvallet, C. (2018) Towards smart port: An application of AIS Data. In: 2018 IEEE 20th International Conference on High Performance Computing and Communications; IEEE 16th International Conference on Smart City; IEEE 4th International Conference on Data Science and Systems (HPCC/SmartCity/DSS). New York: IEEE